HHS Public Access

Author manuscript

Neuron. Author manuscript; available in PMC 2024 June 07.

Published in final edited form as:

Neuron. 2023 June 07; 111(11): 1795–1811.e7. doi:10.1016/j.neuron.2023.03.014.

Oxytocin promotes prefrontal population activity via the PVN-PFC pathway to regulate pain

Yaling Liu[1], **Anna Li**[1,2], **Chloe Bair-Marshall**[3,4,5,6], **Helen Xu**[1,2], **Hyun Jung Jee**[1,2], **Elaine Zhu**[1,2], **Mengqi Sun**[1], **Qiaosheng Zhang**[1,2], **Arthur Lefevre**[7,#], **Zhe Sage Chen**[4,5,8], **Valery Grinevich**[7], **Robert C. Froemke**[3,4,5,6], **Jing Wang**[1,2,4,5,9,*]

[1]Department of Anesthesiology, Perioperative Care and Pain Medicine, New York University Grossman School of Medicine, New York, NY, USA.

[2]Interdisciplinary Pain Research Program, New York University Langone Health, New York, NY, USA.

[3]Skirball Institute for Biomolecular Medicine, New York University Grossman School of Medicine, New York, NY, USA.

[4]Department of Neuroscience and Physiology, New York University Grossman School of Medicine, New York, NY, USA.

[5]Neuroscience Institute, New York University Grossman School of Medicine, New York, NY, USA.

[6]Department of Otolaryngology, New York University Grossman School of Medicine, New York, NY, USA.

[7]Department of Neuropeptide Research in Psychiatry, Central Institute of Mental Health, Medical Faculty Mannheim, University of Heidelberg, Mannheim, Germany.

[8]Department of Psychiatry, New York University Grossman School of Medicine, New York, NY, USA.

[9]Lead contact

SUMMARY

Neurons in the prefrontal cortex (PFC) can provide top-down regulation of sensory-affective experiences such as pain. Bottom-up modulation of sensory coding in the PFC, however,

*Correspondence: jing.wang2@nyumc.org.

#Current address: Cortical Systems and Behavior Laboratory, University of California San Diego, USA

AUTHOR CONTRIBUTIONS

Y.L., H.X., H.J.J., E.Z., and M.S. performed the behavior experiments. Y.L., A.L., H.J.J., and Q.Z. performed the *in vivo* calcium imaging experiments. C.B.M. performed patch clamp recordings. Y.L., A.L., H.X., C.B.M., Q.Z., Z.S.C., R.C.F. and J.W. analyzed data. J.W. designed the experiments and supervised the study with assistance from Z.S.C. and R.C.F. A.L. and V.G. provided the oxytocin promoter viruses and consultation for their usage, as well as commented on the manuscript. J.W. wrote the manuscript, with help from other authors.

DECLARATION OF INTERESTS

The authors declare no competing interests.

remains poorly understood. Here we examined how oxytocin signaling from the hypothalamus regulates nociceptive coding in the PFC. *In vivo* time-lapse endoscopic calcium imaging in freely-behaving rats showed that oxytocin selectively enhanced population activity in the prelimbic PFC in response to nociceptive inputs. This population response resulted from reduction of evoked GABAergic inhibition and manifested as elevated functional connectivity involving pain-responsive neurons. Direct inputs from oxytocin-releasing neurons in the paraventricular nucleus of the hypothalamus (PVN) are crucial to maintaining this prefrontal nociceptive response. Activation of the prelimbic PFC by oxytocin or by direct optogenetic stimulation of oxytocinergic PVN projections reduced acute and chronic pain. These results suggest that oxytocinergic signaling in the PVN-PFC circuit constitutes a key mechanism to regulate cortical sensory processing.

eTOC Blurb

Liu et al. reveal that oxytocin enhances the population nociceptive response in the prelimbic prefrontal cortex (PL-PFC) to inhibit acute and chronic pain in rats. The oxytocinergic projection from the paraventricular nucleus of the hypothalamus (PVN) to the PL-PFC regulates pain by altering the excitation-inhibition balance in the PL-PFC.

INTRODUCTION

The prefrontal cortex (PFC) is a command center for top-down regulation of sensory inputs.[1] Activation of key components of the PFC has been reported to suppress pain.[2,3,4,5,6,7,8] Individual neurons in the PFC can be recruited into a specific functional neural circuit in a context-dependent manner.[9] Studies have demonstrated roles of glutamate, endocannabinoid, and cholinergic signaling in prefrontal nociceptive processing,[8,10,11,12] and mapped efferent projections from the PFC.[5,6,13,14,15,16] In contrast, bottom-up mechanisms of neurohormonal and subcortical modulation of prefrontal nociceptive processing remain poorly known.

Oxytocin is a peptide hormone implicated in socially driven behaviors including mating and nursing,[17,18,19,20] as well as in stress and fear behaviors.[21,22,23] Oxytocin is synthesized by neurons from the paraventricular nucleus (PVN) and supraoptic nucleus (SON) of the hypothalamus,[24,25,26] and it targets a number of neural structures, including the neocortex.[27,28] Its role in nociceptive processing has been studied in spinal and peripheral neurons,[29,30,31,32,33] and subcortical brain structures.[22,34,35,36] Neurons in the PFC express a high number of oxytocin receptors and receive direct inputs from the PVN.[22,37,38] However, the role of oxytocin in prefrontal nociceptive processing remains largely unknown.[39]

Here, we studied the role of oxytocinergic projection from the PVN on the neuronal activity of the prelimbic PFC (PL-PFC). We found that oxytocin increased the population nociceptive response in the PL-PFC, likely resulting from alterations in local excitation-inhibition (E/I) balance. Further, we found that presynaptic PVN inputs strongly shaped the nociceptive response in PFC neurons. Finally, oxytocin, either administered locally or directly through activation of the axon terminals of PVN neurons in the PL-PFC, reduced pain behaviors. These results support a key subcortico-cortical pathway for endogenous

pain regulation and demonstrate the importance of neurohormonally driven bottom-up modulation of cortical sensory coding.

RESULTS

Oxytocin enhances the nociceptive response in the PL-PFC

To evaluate the anti-nociceptive effects of oxytocin in rats, we measured withdrawal latency in response to a noxious thermal stimulus using the Hargreaves test (Figure 1A). We found that rats after systemic (intraperitoneal) delivery of oxytocin (1 mg/kg) showed increased withdrawal latency from baseline, compared with saline control (Figure 1B), indicating anti-nociceptive effects.

Next, we tested the effect of oxytocin on the nociceptive response in the PL-PFC, using time-lapse calcium (Ca^{2+}) imaging in awake, freely-behaving rats. We injected GCaMP6f into the PL-PFC, and mounted a single-photon miniscope with a GRIN lens to track Ca^{2+} activity within CAMKII-expressing pyramidal neurons (Figures 1C and 1D). Within each imaging session, we measured Ca^{2+} activity both before and after administering a peripheral stimulus, a noxious 27 G pin prick (PP), to the paw contralateral to the implanted lens, and we identified population response to this noxious stimulus (Figures 1E–1G), compatible with earlier findings.[9]

To test how oxytocin modulates neuronal activity within the PL-PFC, we compared the peak fluorescence within PL-PFC in response to PP before and after oxytocin administration (Figures 1H–1J and S1A). We found an increase in the average peak Ca^{2+} activity after oxytocin administration in pain-responsive neural populations or regions of interest (ROIs) (Figure 1J). This increase in ΔF, which indicates that neurons likely fire more action potentials in the presence of oxytocin, was not observed after saline (control) injection (Figures 1K–1M, S1B, S2).

Oxytocin signaling in the PL-PFC inhibits acute pain

Having demonstrated that oxytocin signaling enhances the population nociceptive response in the PL-PFC, we examined how it might regulate pain behaviors. We delivered oxytocin through cannulas placed in the PL-PFC and measured withdrawal latency (Figure 2A). We injected two different doses of oxytocin, and found that both doses, compared with saline (control), prolonged withdrawal latency, with the higher dosage producing a greater effect (Figure 2B).

Next, we assessed the anti-aversive effects of oxytocin using a well-established two-chamber conditioned place aversion (CPA) assay.[6,40,41] We administered oxytocin or saline intracranially to the rats prior to the CPA assay (Figure 2C). During the preconditioning phase of the test, rats were allowed to move freely between two chambers. In the conditioning phase, one of the chambers was paired with repeated noxious stimulation (PP) of the hind paw, whereas the opposite chamber was not associated with any noxious stimuli (NP) (Figure 2D). During the testing phase, rats were allowed to move freely again without any peripheral stimulus.

When only saline was delivered to the PL-PFC, rats displayed an aversion to the PP-paired chamber (Figure 2E). In contrast, rats that received oxytocin did not exhibit aversion to the chamber paired with PP (Figure 2F), indicating that oxytocin in the PL-PFC reduced pain aversion. To quantitate these results, we compared the CPA scores of saline-treated rats with oxytocin-treated rats. The CPA score was computed by subtracting the amount of time rats stayed in the PP-paired chamber during the testing phase from the time in the preconditioning phase. A higher CPA score indicates greater aversion.[6,40,41] The CPA score was lower for the oxytocin group, supporting oxytocin's anti-aversive effect (Figure 2G). In contrast to its pain-regulatory effects, oxytocin did not alter locomotor behaviors (Figure S3).

Oxytocin in the PL-PFC inhibits chronic inflammatory pain

We next tested the role of prefrontal oxytocin signaling in regulating chronic pain. We injected Complete Freund's Adjuvant (CFA) subcutaneously into the hind paws of rats to induce persistent inflammatory pain (Figure 3A), as shown by mechanical allodynia (Figure 3B). Oxytocin delivery into the PL-PFC, however, reduced mechanical allodynia (Figure 3C).

In addition to peripheral hypersensitivity, another hallmark feature of chronic pain is spontaneously occurring pain in the absence of external stimuli. Thus, we performed a conditioned place preference (CPP) assay on CFA-treated rats to examine how oxytocin in the PL-PFC regulates spontaneous or tonic pain.[5,6,42,43] During the conditioning phase, rats were allowed to move freely without external stimuli, and we paired one chamber with intra-PFC oxytocin infusion and the other chamber with saline infusion, separated by 5 hours (Figure 3D). Each conditioning session lasted 30 minutes, and we conditioned rats for four consecutive days. During the testing phase, we found that CFA-treated rats preferred the chamber associated with oxytocin (Figure 3E). Control pain-free rats with saline injection into hind paws did not demonstrate a preference for oxytocin (Figure 3F). To further quantify this anti-aversive effect of oxytocin, we computed a CPP score by subtracting the amount of time a rat spent in the oxytocin-associated chamber during the preconditioning phase from the time spent in the testing phase.[5,44] A higher CPP score indicates a greater anti-aversive effect. We found that oxytocin treatment indeed produced a high CPP score in CFA-treated rats (Figure 3G). These results indicate that oxytocin signaling in the PL-PFC inhibited spontaneous pain induced by chronic pain.

Inputs from the PVN maintain the tone of nociceptive response in the PL-PFC

While oxytocin released from the hypothalamus could arrive at the PL-PFC via systemic pathways, there is a possibility for a direct pathway from the PVN to the PL-PFC.[22,37,38] To investigate this direct pathway, we first validated the anatomic projection from the PVN to PL-PFC. We injected OTp-Venus into the PVN of rats (Figures 4A and 4B),[22] and immunohistochemistry staining confirmed fluorescence in axons of OTp neurons within the PL-PFC (Figure 4C).

To assess the function of the PVN-PFC projection, we used Designer Receptors Exclusively Activated by Designer Drugs (DREADD) to test whether chemogenetic inactivation of

the PVN could alter the nociceptive response within the PL-PFC. We injected hM4D(Gi) DREADD into the PVN, and delivered clozapine N-oxide (CNO) to activate the inhibitory hM4D(Gi) DREADD within the PVN. As a control, we injected OTp-Venus into the PVN. We then measured Ca^{2+} activity in response to PVN inactivation (Figure 4D). Specifically, we imaged Ca^{2+} activity in response to PP, delivered to the contralateral paw of awake, freely-behaving rats (Figures 4E and 4F). We found that pain-responsive neuronal ROIs in the PL-PFC, following CNO injection, exhibited a decrease in mean peak Ca^{2+} activity in response to PP (Figures 4G and 4H) Control rats, however, exhibited no such changes in activity (Figure 4I). These results indicate that inactivation of the PVN decreases the nociceptive response of the PL-PFC, and thus oxytocinergic neurons in the PVN likely play a key role in maintaining the tone of prefrontal nociceptive response.

Oxytocin released from the axonal terminals of PVN neurons alters the excitation-inhibition balance in the PL-PFC

The decreased prefrontal activity revealed by *in vivo* imaging experiments might be either a direct or indirect result of PVN inhibition. To further dissect the role of the direct projection from the oxytocinergic neurons within the PVN to the PL-PFC, we made whole-cell recordings from brain slices of adult rats expressing OTp-ChR2-mCherry in the PVN (Figure 5A). Stimulation of PVN neurons using blue light pulses resulted in a significant reduction in inhibitory postsynaptic currents (IPSCs) in PL-PFC neurons (Figures 5B–G, blue), but no significant reduction in excitatory postsynaptic currents (EPSCs) (Figures 5B–D, H-J, green). This effect of PVN stimulation was blocked by the addition of 1 μM of the specific oxytocin receptor antagonist (OTA) to the bath,[45,46] demonstrating that this effect depends on oxytocin release from PVN terminals and subsequent activation of cortical oxytocin receptors (Figures 5F,G). Together, these results indicate that oxytocin release from PVN terminals could directly enhance the nociceptive response in PL-PFC neurons by reducing evoked inhibition, thereby enhancing the impact of evoked excitatory inputs.

Oxytocin enhances resting-state functional connectivity within the PL-PFC

To further understand the effect of oxytocin at the network level, we adopted the graph-theoretic functional connectivity analysis to examine the relationships amongst PFC neurons from distinct functional groups.[9]

First, we applied a nonnegative spike deconvolution method to infer the proxy of spiking activities from preprocessed Ca^{2+} fluorescence time series of prefrontal ROIs.[47] We then used this spiking activity proxy to compute scale-invariant cross-correlation between neuronal ROIs for graph generation, with each node representing one putative neuronal ROI and the edge representing the strengths of significant cross-correlation (Figure 6A). To quantitatively assess functional connectivity between relevant PFC neuronal populations before (pre) and after (post) administration of oxytocin, we proportionally subsampled a subset of pain-responsive and non-responsive neuronal ROIs in each set of pre and post recording sessions while accounting for their firing rates (see Methods).

We adopted a previously established procedure to calculate two graph-network statistics: the betweenness centrality (C_B) and degree centrality (C_D), to determine the role

of pain-responsive neurons in processing nociceptive information within the PL-PFC.[9] Computationally defined neurons are modeled as nodes within the PL-PFC neural network. Betweenness centrality of the graph is defined as the volume of shortest paths that travel through a given node, and it measures the importance of the node as a hub for information flow within the overall prefrontal network (Figure 6B).[48,49] Degree centrality is a measure of the number of edges connected to a given node, and indicates the importance of the node as a functional hub to other nodes within the network (Figure 6C).[48,49] Although few neurons consistently responded to noxious inputs across different recording sessions (Figures S4A–S4B), the average firing rate of neurons remained remarkably stable across baseline sessions (Figure S4C). Importantly, while the identity of pain-responsive neurons may differ across sessions, graph-theoretic metrics of functional connectivity remained stable during the resting state (Figures S5A–S5D), which is consistent with previous work.[9]

We evaluated the functional connectivity using the betweenness and degree centrality metrics in graphs generated from subsampled neuronal ROIs before and after oxytocin treatment (Figures 6D and 6E). After oxytocin treatment, we observed a significant increase in the betweenness centrality of pain-responsive nodes (Figure 6F). In contrast, non-responsive nodes did not exhibit a discernable response to oxytocin (Figure 6G). A similar increase was also observed in degree centrality among pain-responsive neurons, but not among non-responsive neurons (Figures 6H and 6I). Changes induced by oxytocin were not found with saline treatment (Figures S6). These findings indicate that oxytocin improves the functional connectivity between pain-responsive neurons and other neurons within the local PFC network to increase the role of pain-responsive neurons within a network.

Direct projection from oxytocin-releasing neurons in the PVN to the PFC regulates acute pain

Having shown the role of direct inputs from OTp-expressing neurons in the PVN in maintaining the nociceptive response in the PL-PFC, we then studied how this projection could regulate pain behaviors. We injected OTp-ChR2-mCherry or control OTp-Venus viral vector in the PVN, and implanted optic fibers in the PL-PFC to specifically target axon terminals of oxytocin-releasing neurons projecting from the PVN (Figure 7A).

First, we tested whether optogenetic activation of the OTp-expressing neurons within the PL-PFC could produce anti-nociceptive effects using the Hargreaves test (Figure 7B). We found that light activation of the axon terminals of these OTp-expressing neurons within the PL-PFC increased the withdrawal latency in ChR2-expressing rats (Figure 7C), indicating an inhibition of sensory pain symptoms.

Next, we investigated the anti-aversive role of this projection using the CPP assay. In the conditioning phase, one chamber was paired with PP and optogenetic activation of the axon terminals of OTp neurons in the PL-PFC, and the other chamber was paired with PP without optogenetic stimulation (Figure 7D). The ChR2-expressing rats preferred activation of the PVN-PFC projection (Figure 7E), in contrast to control rats (Figure 7F). A comparison of the CPP scores confirms that activation of the OTp neurons in the PFC reduces pain aversion (Figure 7G). When we performed the optogenetic CPP assay without the administration of

noxious stimuli (Figure 7H), rats exhibited no preference for activation of the PVN-PFC circuit (Figure 7I).

To further confirm that the PL-PFC is indeed an important target of the PVN oxytocinergic projection, we tested whether optogenetic inhibition of the PL-PFC would block the anti-nociceptive effects of the PVN-PFC pathway. We injected ChR2 into the PVN and halorhodopsin (NpHR) into the PL-PFC, with optic fibers implanted in both regions (Figure 7J). We then conducted a CPP assay by conditioning rats in one chamber paired with PP and simultaneous activation of the PVN and inhibition of the PL-PFC, and the opposite chamber paired with PP without optogenetic modulations (Figure 7K). Rats showed no preference for either chamber, suggesting that direct inhibition of the PL-PFC removed the anti-aversive effects of PVN activation (Figure 7L). When we compared the CPP score for the effect of this simultaneous activation of PVN and inhibition of PL-PFC with CPP score for activation of PL-PFC, we found that inhibition of PL-PFC indeed blocked the pain-relieving effect of PVN activation (Figure 7M). To confirm these results, in the same group of rats that had dual expression of ChR2 in the PVN and NpHR in the PL-PFC, we paired one chamber with PP and simultaneous activation of the PVN and inhibition the PL-PFC, and the other chamber with PP and only activation of the PVN (Figure 7N). Rats preferred the chamber paired with PVN activation (Figure 7O). To further validate these results, we expressed both ChR2 and NpHR in PVN neurons, and inserted optic fibers to either target the PVN neurons directly or the axon terminals of PVN neurons that project to the PL-PFC (Figures S7A). We then conducted CPP assays with PP, by simultaneously activating PVN cell bodies and inhibiting the axon terminals of these cells that project to the PL-PFC in one chamber and delivering no light treatment in the opposite chamber during conditioning (Figure S7B). Rats showed no chamber preference (Figure S7C). Next, we compared simultaneous activation of PVN and inhibition of PVN-PFC projection against only PVN activation (Figure S7D), and rats preferred PVN activation (Figure S7E). Together, these results indicate that the PVN-PFC circuit constitutes a direct pathway for pain regulation.

Oxytocinergic PVN-PFC projection regulates chronic pain

Next, we tested the role of the PVN-PFC projection in regulating chronic pain. We first tested if optogenetic activation of the axon terminals of OTp neurons from the PVN within the PL-PFC could reduce mechanical allodynia in CFA-treated rats (Figures 8A and 8B), and found that ChR2-expressing rats demonstrated an increased withdrawal threshold (Figure 8C).

Next, we studied how activation of the PVN-PFC pathway affects chronic pain aversion using a CPP assay. In the conditioning phase, one chamber was paired with repeated administration of an allodynia-inducing mechanical stimulus (6g vF) to the CFA-treated paw and optogenetic activation of PVN-PFC circuit (Figure 8D). The opposite chamber was paired with the allodynic stimulation without light treatment. The ChR2-expressing rats demonstrated preference for the chamber paired with light treatment (Figure 8E). In contrast, control (Venus-expressing) rats did not show a preference (Figure 8F). The CPP scores further quantitated the anti-aversive effects of the PVN-PFC projection (Figure 8G).

We used a CPP assay to investigate whether oxytocin signaling in the PVN-PFC pathway could also inhibit spontaneous pain in CFA-treated rats. During a 30 min conditioning phase, one chamber was paired with light treatment, and the other chamber was paired with no treatment (Figure 8H). No peripheral stimulus was given in either chamber. ChR2 rats, but not control rats, showed preference for the light-paired chamber (Figure 8I, 8J). A higher CPP score for the ChR2 rats further validated that activation of the OTp axon terminals in the PL-PFC inhibited spontaneous pain (Figure 8K). To confirm these findings, we repeated this tonic pain assay using rats that had undergone spared nerve injury (SNI) surgery to model neuropathic pain (Figure 8L). ChR2 rats that received SNI treatment also preferred the chamber paired with optogenetic activation of the PVN-PFC projection (Figure 8M), further validating the impact of oxytocin signaling in the PVN-PFC circuit on the regulation of chronic pain.

DISCUSSION

In this study, we found that oxytocin signaling in the PL-PFC enhances the population activity in response to nociceptive inputs through alteration of the E/I balance, and that such signaling can be mediated locally by oxytocinergic neurons from the PVN that project directly into the PL-PFC. Finally, oxytocin signaling via this PVN-PFC projection regulates acute and chronic pain.

A recent study identified population response in the PL-PFC that underlies nociceptive regulation.[9] Our current study showed that oxytocin signaling can modulate this population response. The modification of population responses in the cortex may thus be an important mechanism for oxytocin to exert behavioral control. A key finding in our study is that direct activation of the axonal terminals of oxytocinergic neurons from the PVN not only enhances PFC function, but also regulates pain. These results imply that oxytocin regulation of cortical function can be highly localized and pathway specific. The PFC, as the brain's command center, needs to respond rapidly to a variety of sensory and affective cues. Direct projection from the PVN allows oxytocin to locally modify the response of PFC neurons to a contextual cue in an anatomically and temporally specific manner.

To analyze the impact of oxytocin signaling in the PFC on pain regulation, we have conducted assays for acute pain (Hargreaves' test and CPA/CPP in the context of PP) as well as chronic pain (mechanical allodynia and CPA/CPP using vF filaments). While noxious stimuli are not interchangeable, these assays demonstrate that oxytocin signaling can reduce both sensory and affective components of pain. For example, whereas PPs were used to provide noxious stimuli during our neural imaging studies, mechanical allodynia provides a standard assay for sensory pain behaviors. At the same time, the use of PPs in CPA assays allowed us to further assess mechanical pain responses. Overall, findings on these behavioral tests are compatible with the anti-nociceptive function of PL-PFC in previous studies.[2,4,5,8,13,14,44,50] The PFC has descending projections to the spinal cord to inhibit ascending nociceptive signals.[5,14,51] It can also project to other cortical and subcortical areas to exert central anti-aversive effects.[15] Thus, oxytocin signaling in the PFC has multiple output circuit mechanisms for regulating sensory and affective components of pain.

Acute pain stimuli can trigger oxytocin release in both central and peripheral neurons,[29,32,52] and evoked pain or discrete spontaneous pain episodes in chronic pain conditions may follow a similar mechanism to trigger oxytocin signaling in the PVN. The PFC is known as a center for descending inhibition, and thus oxytocinergic signaling in this region may serve as an important response to pain and an endogenous pain regulatory mechanism. Here we found that oxytocin triggers rapid and relatively sustained reduction in cortical IPSCs, resulting in synaptic disinhibition of the PL-PFC. The timing of this sustained cortical disinhibition, meanwhile, matches the anti-nociceptive effects of oxytocin within the PFC. In both the hippocampus and auditory cortex, similar long-term modifications of the E/I balance have been observed to enhance pyramidal neuronal spiking to give rise to memory-based and maternal care behaviors.[18,53,54] Thus, modification of the synaptic E/I balance may indeed be a general feature for oxytocin signaling in the cortex.

In addition to synaptic modification, our graph theoretic analysis indicates that oxytocin can also reshape local pain circuits. Analysis of functional connectivity has long provided a basis for understanding population-level responses to sensory inputs in various neuropsychiatric conditions,[55,56,57,58] including chronic pain.[55,59] Recent development of graph-theoretic approaches has enabled functional connectivity analysis at the level of local networks.[9,60,61] Graph-network features such as betweenness centrality and degree centrality have been used to identify neural hubs that coordinate network information flow.[62,63,64,65] Pain-responsive neurons in the PFC have been shown to demonstrate high betweenness centrality and degree centrality and thus serve as critical hubs for organizing network response in the presence of nociceptive inputs.[9] The PFC likely employs a dynamic coding mechanism that is based on a recruited subnetwork, rather than a fixed neuronal population with unimodal selectivity.[9] This population-coding mechanism allows the PFC to supervise multiple behavioral tasks with a high degree of flexibility and efficiency.[66,67,68] Here we found that oxytocin signaling significantly increases key features of functional connectivity to reshape the circuit response in the PFC to nociceptive inputs at the population level.

In our *in vivo* analysis, we delivered GCaMP6f using a CaMKII promoter which primarily targeted pyramidal neurons in the PL-PFC. There is a small possibility, however, that some of the imaged neurons may be interneurons. Although our slice recording experiments validated the function of oxytocin signaling in synaptic excitation and inhibition, we did not investigate in detail the contribution of different classes of interneurons in our *in vivo* studies in rats. A large number of oxytocin receptor expressing cells in the cortex and hippocampus have been found to be somatostatin or parvalbumin positive interneurons, and oxytocin is known to specifically target these neurons, leading to increased spontaneous transmitter release that depletes their vesicle pool.[18,28,53] The complex interplay between interneurons and excitatory neurons likely has a key role in the nociceptive processing in the PFC, and future studies are needed to directly analyze interneuronal activity for deeper understanding of the diverse roles of oxytocin signaling. Meanwhile, approximately 60% of the neurons we imaged were from layers 5 and 6, whereas the rest of the neurons were from superficial layers. Cheriyan and Sheets previously reported layer-specific roles for nociceptive processing in the PL-PFC,[13] and thus future studies to specifically targeting layer 2/3 vs layer 5 will provide further details on cortical nociceptive processing.

Several behavioral states are known to trigger the endogenous release of oxytocin, such as stress.[69,70,71,72,73,74] Oxytocin release triggered by external stimuli and/or internal affective state will likely result in widespread activation or inhibition of neural functions. Our results here demonstrate a relatively specific role for oxytocin signaling in the PFC on the regulation of chronic pain, and they also suggest a potential mechanism that tonic inputs into the PFC from the paraventricular oxytocinergic neurons may be altered and in turn contribute to prefrontal deactivation frequently found in chronic pain states.[7,8,9,12,75,76] Future enquiries into such circuit mechanisms can provide additional insights on neurohormonal regulation of cortical pain processing. Future studies are also needed to further establish the physiological role of oxytocin as a mediator of endogenous analgesia, including studies to systematically investigate the impact of oxytocin on response to various modalities of noxious stimulations, as well as studies in both male and female sexes. Further, to completely unlock the therapeutic potential of oxytocin, work is needed to fully understand how systemic delivery of oxytocin can achieve pain-relieving effects through activity in both peripheral and central nervous systems.

In summary, we have shown that oxytocin signaling can shape the E/I balance to modulate the nociceptive processing in the PL-PFC. The impact of oxytocin on nociceptive processing can be mediated locally by neurons from the PVN in the hypothalamus that project directly into the PL-PFC. These results provide an important subcortico-cortical pathway for pain regulation, and more generally, they demonstrate the significance of bottom-up signaling in shaping higher-cortical regulation of sensory-affective behaviors.

STAR METHODS

RESOURCE AVAILABILITY

Lead contact—Further information and requests for resources should be directed to and will be fulfilled by the lead contact, Jing Wang (jing.wang2@nyulangone.org).

Materials availability—This study did not generate new unique reagents.

Data and code availability

- All data reported in this paper will be shared by the lead contact upon request.
- All original code has been deposited at Zenodo and is publicly available as of the date of publication. DOIs are listed in the key resources table.
- Any additional information required to reanalyze the data reported in this paper is available from the lead contact upon request.

EXPERIMENTAL MODEL AND SUBJECT DETAILS

Animals—All procedures were performed in accordance with the New York University School of Medicine (NYUSOM) Institutional Animal Care and Use Committee (IACUC) guidelines to ensure minimal animal use and discomfort, as consistent with the National Institute of Health (NIH) *Guide for the Care and Use of Laboratory Animals*. Male Sprague-Dawley rats were purchased from Taconic Farms (Albany, NY) and were housed

at the vivarium facility in the NYU Langone Science Building under controlled humidity, temperature, and 12 h (6:30 AM to 6:30 PM) light-dark cycle. Food and water were available to the rats *ad libitum*. Animals weighed between 250–300 g upon arrival at the animal facility. The animals were given 10–14 days to adjust to the new environment before participating in behavioral experiments.

METHOD DETAILS

Virus construction and packaging—Recombinant adeno-associated virus (AAV) vectors, packaged at Addgene viral vector manufacturing facilities, were serotyped with AAV1 coat proteins. pENN.AAV1.CamkII.GCaMP6f.WPRE.SV40 and AAV1.CaMKIIa.eNpHR.3.0.EYFP viral titers were approximately 5×10^{12} particles per milliliter. OTp-ChR2-mCherry, OTp-Venus, and OTp-hM4D(Gi)-mCherry were donated by Dr. Grinevich (Germany). The hM4D(Gi) DREADD used is a Gi-coupled receptor that is activated by Clozapine-N-oxide (CNO).

Intracranial viral injections and optic fiber implantation—As described in previous studies,[5] rats were anesthetized with 1.5–2% isoflurane. Rats were bilaterally injected with 0.65 μL viral vectors at a rate of 0.1 μL/20 s using a 26G 1 μL Hamilton syringe at anteroposterior (AP) −1.8 mm, mediolateral (ML) ±0.3 mm, and dorsoventral (DV) −7.6 mm. Post viral injection, the microinjection needles were left in place for 10 min before they were raised 0.5 mm, allowing viral particles to diffuse and minimizing particle dispersion along the injection tract. The microneedle was held in place for an additional 5 min before being slowly raised from the brain. Rats that received bilateral virus injections, were then implanted unilaterally with 200 μm optic fibers held in 2.5 mm ferrules (Thorlabs) in the PL-PFC at AP +2.9 mm, ML ±1.6 mm, and DV −3.0 mm, with the tips angled at 17° towards the midline. The fibers and ferrules were secured using dental acrylic. For the gradient-index (GRIN) lens implantation, 0.65 μL viral vectors of GCaMP6f virus were injected unilaterally to PL-PFC at AP +2.9 mm, ML ±1.6 mm, and DV −3.7 mm, with the tips angled at 17° towards the midline.

Drugs—0.1 mL of Complete Freund's Adjuvant (CFA) (*Mycobacterium tuberculosis*, Sigma-Aldrich) was suspended in a 1:2 oil:saline emulsion, then injected subcutaneously into the plantar surface of the hind paw to induce persistent inflammatory pain. CFA was injected contralateral to the paw peripherally stimulated with pin prick (PP) or von Frey filament (vF). Oxytocin (Abcam) was suspended in 0.9% saline with a dose of 1 mg/kg for systemic injection. Oxytocin was suspended again in 0.9% saline for final concentrations of 1.0 μg/μL and 0.5 μg/μL for intra-PL-PFC infusions.[77,78] Clozapine N-oxide (CNO) was suspended in 0.9% saline for a final concentration of 1g/mL and was intraperitoneally injected with a dose of 3 mg/kg.

Gradient-index lens implantation and mounting—Rats were stereotaxically implanted with the gradient-index (GRIN) lens (1.0 mm diameter, ~9.0 mm length, Inscopix) at AP +2.9 mm, ML ±1.6 mm, and DV −3.5 mm, with the tips angled at 17° towards the midline approximately 4–6 weeks following intracranial injections of viral pENN.AAV1.CamkII.GCaMP6f.WPRE.SV40 to the PL-PFC contralateral to the site of

peripheral stimulation. The GRIN lens was placed approximately 100–300 μm above the imaging plane. Silicone elastomer (Kwik-Sil, World Precision Instruments) was used to fill the gap between the placement of the lens and the open craniotomy site. Dental acrylic was used to secure the lenses in place.

Approximately four weeks following lens implantation, rats were anesthetized with 0.5–1% isoflurane prior to inspection for GCaMP6f fluorescence and Ca^{2+} transient activity. The responsiveness of the rats under light anesthesia was confirmed by their paw retractions when pinched. The miniature microscope (nVoke, Inscopix) with an attached baseplate was stereotaxically adjusted relative to the GRIN lens implantation to determine an optimal field of view (FOV) for neural activity imaging. Rats that exhibited neural responses to both auditory (clapping) and sensory (tail pinching) stimuli proceeded to have a baseplate mounted. Afterwards, the anesthesia was raised to 1.5–2% isoflurane. The baseplate was secured using adhesive cement (Metabond Quick! Adhesive Cement System, C&B) and a baseplate cover (Inscopix) was then magnetically attached to the baseplate to protect the GRIN lens when it is not in use.

GRIN lens imaging procedure—The rat was placed within the recording chamber over a mesh table at the start of each imaging session. The miniature microscope was mounted on the baseplate by aligning the recording FOV with the previous session FOV. While the rat was habituating to and freely moving within the chamber without receiving any stimuli from the experimenter, spontaneous neural activity was recorded. Noxious stimulation was delivered to freely moving rats by pricking the plantar surface of the hind paw contralateral to the brain recording site using pin prick (PP) by a 27G needle. Once there was a withdrawal of the paw, noxious stimulation was terminated. Each recording session consisted of 7 trials of peripheral stimulus with inter-trial intervals of approximately 60 s to avoid sensitization to the stimuli. A video camera (HC-V550, Panasonic) recorded the experiments. No physical damage to the paws or behavioral was observed.

Imaging experiments involving the oxytocin/saline condition were performed 15–20 min after oxytocin/saline systemic (intraperitoneal) injection. Experiments involving the activation of the hM4D(Gi) DREADD by CNO administration were performed 1 hour after systemic CNO injection.

GRIN lens data acquisition and preprocessing—The miniature fluorescent microscope videos were recorded at a frame rate of 20 Hz. Post-acquisition, raw videos were downsampled spatially by a binning factor of 4 (16x spatial downsample) and temporally by a binning factor of 2 (down to 10 frames per second) using Inscopix Data Processing Software (Inscopix). The videos were motion-corrected relative to a single reference frame to match the XY positions of each frame throughout the video using Inscopix Data Processing Software. The motion-corrected 10 Hz video of raw Ca^{2+} activity was saved as a .TIFF file for neural response analysis. To estimate temporally constrained instances of calcium activity for each neuronal region of interest (ROI), Ca^{2+} signals were extracted using modified constrained non-negative matrix factorization scripts (CNMF_E) in MATLAB.[79,80,81] Cross-session neuronal regions of interest (ROIs) were matched using CellReg by comparing contours and centroid locations.[82]

Cannula implantation and intracranial injection—For cannula implantations, rats were anesthetized with isoflurane (1.5–2%) and underwent the procedure as described previously.[83] Rats were stereotaxically implanted with two 26G guide cannulas (P1 Technologies, Roanoke, VA) bilaterally in the PL-PFC at AP +2.9 mm, ML ±1.6 mm, and DV −2.2 mm, with the tips angled at 20° towards the midline. Cannulas were secured in place by dental acrylic and kept clean and unobstructed for injections using occlusion stylets. For intracranial injections, solutions were loaded into 30 cm long tubes of PE-50 attached at one end to a 10 μL Hamilton syringe filled with distilled water. The other end of the tube was attached to a 33G cannula injector, which extended 1 mm past the implanted guides. Injections took place over the course of 120 s at a rate of 0.05 μL per 10 s, and the implants were left in place for 60 s post-injection to allow for diffusion of the solution within the brain. Occlusion stylets were replaced before starting the experiments. Behavior tests were conducted 15–20 min post-injection.

Spared nerve injury (SNI) surgery—As described in previous studies,[84] the rats were anesthetized with 1.5–2% isoflurane. An incision was made on the skin of the rat's right thigh. The biceps femoris muscle was separated through blunt dissection until the sciatic nerve and its three terminal branches (sural, common peroneal, and tibial) are clearly visible. Using nonabsorbent 4–0 silk sutures, the common peroneal and tibial nerves were tied at the proximal point of trifurcation. Another knot was made around these two nerves, distally to the first not. The two nerves were then cut between the knots. The muscle layer was closed with sutures, and the skin was then stapled.

Hargreaves' test (plantar test)—A mobile heat-radiating device with an aperture of 10 mm (37370 plantar test, Ugo Basile) was used to deliver acute thermal stimulation of the plantar surface of the hind paw.[85] The rats were allowed to habituate in a plexiglass chamber placed over a Hargreaves glass table. At least five trials were performed for each testing condition to measure the paw withdrawal latency. This latency was automatically recorded, and the average across the trials for each condition was computed. Trials in which paw withdrawals resulted from locomotion or weight shifting were discarded and repeated. Trials were conducted at approximately 3–5 min intervals. An infrared (IR) intensity of 40 was used to provide the noxious thermal stimulation. Hargreaves' test was conducted approximately 20 min after oxytocin infusions.

Mechanical allodynia test—A Dixon up-down method using von Frey (vF) filaments was performed to measure mechanical allodynia.[83] The rats were placed individually into plexiglass chambers over a mesh table and given 20 min to acclimate. A set of vF filaments with logarithmically incremented stiffnesses were applied to the middle of the plantar surface of the rats' hind paws, and a 50% withdrawal threshold was calculated using the up-down method described previously.[83,84] This test was conducted approximately 20 min after oxytocin infusions.

Conditioned place aversion assay—Conditioned place aversion (CPA) experiments were conducted similarly to those described in previous experiments, in a standard two-compartment apparatus consisting of equally sized compartments connected by an opening

large enough for a rat to freely travel between the two chambers.[2,40,41] Different balm scents were applied to the chamber walls to provide distinguishing contextual clues. The CPA protocol consisted of preconditioning (baseline), conditioning, and testing phases. The preconditioning phase was 10 min, and animals spending greater than 480 s or less than 120 s of the total time in either chamber during this phase were eliminated from further analysis. The rats underwent conditioning immediately after the preconditioning phase. During conditioning (10 min per chamber), one chamber was paired with noxious peripheral stimulus (PP), and the other chamber was paired with no peripheral stimulus. The peripheral stimulus was administered at intervals of 30 s. The order of stimulation was counterbalanced, e.g. half of the rats received peripheral stimulation first, whereas the other half received the control treatment first during the conditioning phase. Chamber pairings were also counterbalanced. No stimulations were given during the testing phase (10 min), and the rats were allowed to move freely between chambers. Movements of the rats in each chamber were recorded by a camera and then analyzed using AnyMaze software. Decreased time spent in a chamber during the testing phase relative to the baseline indicated avoidance (aversion) of that chamber. In contrast, increased time spent in a chamber during the testing phase relative to the baseline indicated decreased aversion to that chamber. A CPA score quantitating the animal's aversion to the treatment was calculated by subtracting the time the animal spent in the treatment chamber associated with PP in the testing phase from the time it spent during the preconditioning phase. A higher CPA score indicated increased pain aversion. This test was conducted approximately 15 min after oxytocin infusions.

Conditioned place preference assay—Conditioned place preference (CPP) experiments were conducted in the same two-compartment apparatus as the CPA experiments. The CPP assays were performed as described previously.[5,6,42,43] The movements of rats in each chamber were automatically recorded by a camera and analyzed using the AnyMaze software. The CPP protocol, modified from King et al.,[43] included preconditioning (baseline), conditioning, and testing phases. For the CPP assay involving intracranial drug delivery, the preconditioning phase began 2 days after CFA/saline injection to the hind paw and was performed across 3 days. During preconditioning, all animals were exposed to the environment with full access to both chambers for 30 min each day. On day 3 of preconditioning, the movement of each rat was recorded for 10 min and analyzed to confirm the absence of any chamber preference during preconditioning. Animals spending more than 480 s or less than 120 s of the total time in either chamber were excluded from further testing or analysis. Following the pre-conditioning phase, the rats were conditioned for 4 days with alternating intracranial bilateral injections into the PL-PFC of either oxytocin (1.0 μg/μL) or the saline control in the morning and afternoon. The oxytocin and the saline injections were paired with opposite chambers. During conditioning (30 min per chamber), rats were placed in the paired chamber. Drug treatments and chamber pairings were counterbalanced, and at least 5 hours separated morning and afternoon sessions. On testing day, no injections were performed, and the animals had free access to both chambers for a total of 10 min. During the testing phase, animal movements were recorded, and the time spent in each chamber was analyzed using the AnyMaze software.

The CPP protocols involving optogenetic stimulation where conducted similarly to the procedure above, but with different chamber treatment pairings and conditioning phase durations. The conditioning phase was conducted on a single day immediately before the testing phase. The conditioning phase for the optogenetic experiments involving a peripheral stimulus lasted 10 minutes per chamber. The conditioning phases for the spontaneous pain experiments were 30 minutes per chamber. Increased time spent in a chamber during the testing phase indicated the animal's preference for that chamber and its paired treatment. A CPP score quantitating the animal's aversion to the treatment was calculated by subtracting the time the animal spent in the treatment chamber in the preconditioning phase from the time it spent during the testing phase. A higher CPP score indicated increased chamber preference.

Multiple experimenters participated in behavioral experiments. One experimenter performed the surgeries and randomly selected the treatment group and the control group of rats. Other experimenters were blinded to the treatment conditions and performed all the behavior tasks. No data was excluded.

Immunohistochemistry—Rats were deeply anesthetized with isoflurane and then transcardially perfused with ice-cold phosphate buffered saline (PBS) and paraformaldehyde (PFA). Post extraction, brains were fixed in PFA overnight and then cryoprotected in 30% sucrose in PBS for 48 hours or until they sank.[5] 20 μm coronal sections were obtained using the Leica CM 3050 S Cryostat (Leica Biosystems), then washed in PBS and coverslipped with Fluoromount mounting medium (Sigma-Aldrich). High resolution images were acquired with a Zeiss LSM 700 confocal microscope (Carl Zeiss).

In vitro* whole-cell recordings—In vitro* recordings were performed in acute slices of PL-PFC prepared from rats previously injected with OTp-ChR2-mCherry. Rats were deeply anesthetized with a lethal dose of intramuscular ketamine (80 mg/kg) and dexmedetomidine (0.250 mg/kg) and decapitated. The brain was rapidly placed in ice-cold dissection buffer containing (in mM): 87 NaCl, 75 sucrose, 2.5 KCl, 1.25 NaH2PO4, 0.5 CaCl2, 7 MgCl2, 25 NaHCO3, 1.3 ascorbic acid, and 10 D-glucose, bubbled with 95%/5% O2/CO2 (pH 7.4). Slices (400–450 μm thick) were prepared with a vibratome (Leica P-1000), placed in warm artificial cerebrospinal fluid (ACSF, in mM: 124 NaCl, 2.5 KCl, 1.5 MgSO4, 1.25 NaH2PO4, 2.5 CaCl2, and 26 NaHCO3) (33–35 °C) for 30 min, and then cooled to room temperature (22–24 °C) for at least 30 min before use. Slices were transferred to the recording chamber and superfused (2.5–3 ml min−1) with oxygenated ACSF at 33 °C.

Whole-cell voltage-clamp recordings were acquired while focal extracellular stimulation (0.5 ms, 5–1000 μA, 5 Hz rate) was applied with a bipolar glass electrode located 100–500 μM from the recording electrode. Patch pipettes (3–8 MΩ) were filled with the following intracellular solution (in mM): 130 Cs-methanesulfonate, 1 QX-314, 4 TEA-Cl, 0.5 BAPTA, 4 MgATP, 0.3 Na-GTP, 10 phosphocreatine, 10 HEPES, pH 7.2. EPSCs were acquired at −70 mV, while IPSCs were acquired from −20 to 0 mV. To assess effects of stimulation on oxytocin release, a stable baseline was established for at least 10 minutes before PVN neurons were stimulated optogenetically with blue light pulse trains (473 nm wavelength, 15 mA light intensity, 5 ms pulse duration, 20 Hz stimulation rate, 1 second long, 60

repeats). Oxytocin antagonism experiments were performed by adding 1 μM of Vasotocin Trifluoroacetate (Bachem: 4015939.0001) to the bath before beginning recording. Access and input resistance were monitored throughout using a brief hyperpolarizing current step, and recordings were excluded from analysis if the access resistance (Ra) changed >20% compared to baseline or rose above 30 MΩ. Cortical regions and layers were identified using IR video microscopy (Olympus) visualized with an Olympus 40 x water-immersion objective with TRITC filter. Data were filtered at 2 kHz, digitized at 10 kHz, and acquired with Clampex 10.7 (Molecular Devices).

***In vivo* optogenetic stimulation—**A 465 nm blue LED (OPT/LED_Blue_Compact_LC_magnetic, Plexon) or a 620 nm orange LED (OPT/LED_Orange_Compact_LC_magnetic, Plexon) was connected to the optic fiber cannula using a mating sleeve (ADAF2, Thorlabs) and a fiber patch cable. The LED was mounted on a carousel commutator (Plexon) using a magnet to allow for free rotation of the animal's head, and was controlled using Transistor-transistor logic pulse generator (OTPG_4, Doric Lenses). The power output of the optic fiber tip was calibrated prior to each experiment. The stimulation parameters for the blue LED's optic fiber were 20 Hz, with 10-ms pulse width and a duration of 10 s. For the orange LED, continuous laser light was delivered with the laser output fluorescence power of 5–6 mW at the fiber tip.

QUANTIFICATION AND STATISTICAL ANALYSIS

Statistical tests—Results were presented as mean ± SEM. To compare mechanical allodynia withdrawal thresholds for CFA-treated and control rats, a two-way ANOVA with repeated-measures and post hoc multiple pairwise comparison Bonferroni tests were used. In the CPA and CPP assays, a two-way ANOVA with repeated-measures and Sidak's multiple comparisons test were used to compare the time spent in each treatment chamber pre and post conditioning (i.e., preconditioning versus testing phase for each chamber). To compare differences within CPA and CPP scores under various testing conditions, a two-tailed unpaired Student's *t* test was used.

When analyzing imaging data, a paired Student's *t* test was used to compare paired neuronal data recorded in a single imaging session. An unpaired Student's *t* test was used to compare unpaired neuronal data recorded in separate sessions. A Fisher's exact test was used to analyze neuron population changes before and after drug administration. A Wilcoxon rank-sum test was used to compare the spontaneous event rates before and after drug administration. Values of *n* and *p* are detailed within the Figure Legends.

To define a neuronal ROI that altered its activity in response to a peripheral stimulus, the following method was used. Peripheral pin prick stimulations were administered to the hind paw, contralateral to the GRIN lens implantation. For each trial, the raw time series was z-scored based on a baseline range of 5 to 3 seconds prior to the stimulation. The z-scored time series from −5 to 5 seconds relative to the stimulus was then binned into 100 ms bins. The 2 s moving window containing the maximum value between 0 to 5 s post-stimulus was used as the post-stimulus value. A one-tailed Wilcoxon rank sum test was performed

between pre- and post-stimulus values for all peripheral stimulations, and the neuronal ROI was considered pain-responsive if $p < 0.025$.

Significance was defined at $p < 0.05$ for all statistical tests used in this study. GraphPad Prism 9 (GraphPad Software) and MATLAB (MathWorks) were used to calculate statistical significance.

Calcium response analyses—Trial-averaged Ca^{2+} fluorescence traces were calculated for individual ROI by z-scoring each trial from −5 to 5 s, with 0 denoting time of peripheral stimulation (i.e. pin prick) which occur 7 times for each imaging session. Each data point in the trial was z-scored by subtracting the mean and dividing by the standard deviation of a baseline period from −5 to −3 s. Z-scored trials were summed, then divided by the total number of trials to produce a single trial-averaged Ca^{2+} fluorescence trace for each ROI. For each session, trial-averaged Ca^{2+} fluorescence traces from individual ROI were summed, then divided by the total number of regions to obtain a single average neuronal activity trace.

The peak Ca^{2+} fluorescence ΔF of a neuron was calculated from the post stimulus range from 0 to 5 s, where 0 denotes time of peripheral stimulation. Each trial was z-scored by subtracting the mean and dividing by the standard deviation of the baseline range from −5 to −3 s before peripheral stimulation and then binned into 100 ms bins. A 2 s moving window was used to calculate each trial's maximum average Ca^{2+} fluorescence. Then the maximum average Ca^{2+} fluorescence was averaged across all trials to produce a single value for the peak post-stimulus activity of a given ROI within each session.

Spontaneous activity between sessions was calculated as the mean event rate, using a similar method as described in previous studies.[86] The baseline for spontaneous activity was recorded over a period of 5 minutes, both before and after oxytocin administration. To remove fluctuations within the baseline recordings, we calculated a sliding median with a window of 40 s, which was then subtracted from the activity trace. Using this processed trace, we identified transient events as peaks that were greater than 2.5 SD above the baseline noise. Peaks with an inter-event time of < 2 s (or 20 frames) were removed. For each neuron, we calculated the mean Ca^{2+} transient event rate during the baseline period. To determine the mean Ca^{2+} transient event rate per neuronal population for each rat, we took the mean spontaneous rate of the neurons. To compare spontaneous event rate before and after oxytocin administration, we calculated the mean spontaneous event rate for all the rats before oxytocin and used this value to normalize the individual event rates for each rat both before and after oxytocin.

Cross-correlation statistics—Raw traces from Inscopix imaging data were extracted with CNMF_E software (https://github.com/zhoupc/CNMF_E). The raw data used is a scaled version of change in peak Ca^{2+} fluorescence (ΔF). Each recording set consists of a baseline (pre) and oxytocin (post) session, recorded before and after intraperitoneal administration of oxytocin. A total of $n = 8$ sets of pre and post sessions were recorded from five rats. Consistency within each recording set was maintained by trimming the length of each time series to the length of the shortest pre-stimulation recording time in a session, or approximately 5 minutes. Each time series was then normalized with the *normalize* function

in MATLAB (MathWorks, Natick, MA). A well-supported spike deconvolution method (https://github.com/zhoupc/OASIS_matlab) was applied to generate representative spiking data from the normalized time series of each neuronal ROI.[47]

The *xcorr* function in MATLAB was then used to calculate a cross-correlation value between the spiking data from two time series. A lag of 10 was used for this function, and the maximum value generated was added to the undirected cross-correlation matrix. The Monte Carlo simulation method was used to determine whether the cross-correlation value was statistically significant. In this statistical method, the first time series was randomly shuffled, and a cross-correlation value was calculated between the shuffled time series and the second time series over 1000 iterations. These 1000 cross-correlation values were then sorted in ascending order. The cross-correlation value from the two original time series was only included in the cross-correlation matrix comprised of statistically significant values if it was greater than the 950^{th} sorted element. This matrix was then used to produce a graph used for network statistics.

Subsampling analysis—As the number of recorded neuronal populations between recording sessions and animals varied, we created a neuronal subsampling procedure to account for this variability in sample sizes of pain-responsive and non-responsive PL-PFC neuronal ROIs. For each set of baseline (pre) and oxytocin (post) recording sessions, we pre-determined the pain-responsive subsample size to be 60% of the number of pain-responsive neuronal ROIs in the session with the smallest number of pain-responsive neuronal ROIs. We then found the average ratio between pain-responsive to nonresponsive neuronal ROIs for both the pre and post session within the set. We chose the non-responsive neuronal ROIs subsample size to maintain this average ratio. For each session, we sorted the total neuronal ROIs based on their mean baseline firing rates. Then, we constructed a cumulative distribution functions (CDFs) for both the pre and post recording sessions. The x-axis of the CDF plot is the range of mean firing rates, and the y-axis is the percentile distribution from 0 to 1. We then used an “inverse transform sampling” strategy to accommodate neuronal populations with divergent firing rates by ensuring a mixture of both high and low firing neuronal populations. Random variables were uniformly drawn from 0 to 1, and then mapped to the firing rate axis using an inverse CDF. This uniform subsampling procedure was used to account for variability in both number of neuronal populations and ratio of pain-responsive neuronal ROIs between recording sessions within a set. We computed the graph-network statistics for each subsample and conducted 100 iterations of this subsampling procedure. The entire subsampling analysis procedure was performed for both pain-responsive and non-responsive groups for each set of pre and post sessions.

Graph-network statistics—Network statistics for each session were analyzed using Gephi (https://gephi.org/), an open-source network and graph analysis software that produces 3D graph visualization. Within the graph visualizations, the neuronal populations within the network were represented by nodes, and the connections between neurons with significant cross-correlations were displayed as edges. We used two metrics to measure functional connectivity: betweenness centrality (C_B), which represents the volume of shortest paths that pass through a given node, and degree centrality (C_D), which represents

the number of edges attached to a node.[48,49] These two network statistics have been used in previous studies to identify putative neurons that function as hubs for information flow within a network.[62,63,64,65] In our study, C_B and C_D were used to illustrate how oxytocin affects the role of pain-responsive neuronal ROIs within a network.

To analyze the change in neural connections before and after oxytocin administration, we took a subsample of the pain-responsive and non-responsive neuronal ROIs for each set of sessions, using the previously mentioned procedure. After a subsample of N neuronal ROIs were obtained, we calculated a corresponding N-by-N cross-correlation matrix, where all values less than 0.1 were removed. The matrix was then converted into a .gdf file summarizing information of the N nodes and $N(N\text{-}1)$ edges of a network which was subsequently used for graph visualization in Gephi. The pain-responsive neurons were always the first nodes entered into the graph and thus were easily located.

Next, we calculated the median network statistic for C_B and C_D of the nodes corresponding to the pain-responsive and non-responsive putatively defined neurons, respectively, using the Gephi software. As we completed 100 iterations of this subsampling procedure for each session, we the calculated the mean of the 100 subsampling medians to obtain a single value for each network statistic per each session. To normalize the C_D, the median degree from each subsampling was divided by (n-1), with n denoting the total number of subsampled putative neurons. This normalization was completed for pain and nonresponsive neurons independently. To calculate relative C_B and C_D, the baseline condition was set to 1, and the mean statistics of the oxytocin condition was rescaled with respect to the baseline. An unpaired Student's t-test was used to test for significant changes in network statistics between baseline and oxytocin conditions.

Supplementary Material

Refer to Web version on PubMed Central for supplementary material.

ACKNOWLEDGMENTS

The work was supported by NIH grants GM115384 (J.W.), NS121776 (J.W. and C.Z.), U19 NS107616 (R.C.F.), Natural Sciences and Engineering Research Council of Canada Postgraduate Scholarship-Doctoral (C.B.M.), and the German Research Foundation (DFG) grants GR 3619/13–1, GR 3619/15–1, GR 3619/16–1, 3619/19–1 and SFB Consortium 1158–2 (V.G.). A.L. is a recipient of Marie Curie-Skladowska fellowship.

INCLUSION AND DIVERSITY

One or more of the authors of this paper self-identifies as a gender minority in their field of research. One or more of the authors of this paper self-identifies as a member of the LGBTQIA+ community. While citing references scientifically relevant for this work, we also actively worked to promote gender balance in our reference list.

REFERENCES

1. Salzman CD, and Fusi S (2010). Emotion, cognition, and mental state representation in amygdala and prefrontal cortex. Annu Rev Neurosci 33, 173–202. 10.1146/annurev.neuro.051508.135256. [PubMed: 20331363]

2. Dale J, Zhou H, Zhang Q, Martinez E, Hu S, Liu K, Urien L, Chen Z, and Wang J (2018). Scaling Up Cortical Control Inhibits Pain. Cell Rep 23, 1301–1313. 10.1016/j.celrep.2018.03.139. [PubMed: 29719246]
3. Hardy SG (1985). Analgesia elicited by prefrontal stimulation. Brain Res 339, 281–284. [PubMed: 4027626]
4. Kiritoshi T, Ji G, and Neugebauer V (2016). Rescue of Impaired mGluR5-Driven Endocannabinoid Signaling Restores Prefrontal Cortical Output to Inhibit Pain in Arthritic Rats. J Neurosci 36, 837–850. 10.1523/JNEUROSCI.4047-15.2016. [PubMed: 26791214]
5. Lee M, Manders TR, Eberle SE, Su C, D'Amour J, Yang R, Lin HY, Deisseroth K, Froemke RC, and Wang J (2015). Activation of corticostriatal circuitry relieves chronic neuropathic pain. J Neurosci 35, 5247–5259. 10.1523/JNEUROSCI.3494-14.2015. [PubMed: 25834050]
6. Martinez E, Lin HH, Zhou H, Dale J, Liu K, and Wang J (2017). Corticostriatal Regulation of Acute Pain. Front Cell Neurosci 11, 146. 10.3389/fncel.2017.00146. [PubMed: 28603489]
7. Talay RS, Liu Y, Michael M, Li A, Friesner ID, Zeng F, Sun G, Chen ZS, Zhang Q, and Wang J (2021). Pharmacological restoration of anti-nociceptive functions in the prefrontal cortex relieves chronic pain. Prog Neurobiol 201, 102001. 10.1016/j.pneurobio.2021.102001. [PubMed: 33545233]
8. Zhang Z, Gadotti VM, Chen L, Souza IA, Stemkowski PL, and Zamponi GW (2015). Role of Prelimbic GABAergic Circuits in Sensory and Emotional Aspects of Neuropathic Pain. Cell Rep 12, 752–759. 10.1016/j.celrep.2015.07.001. [PubMed: 26212331]
9. Li A, Liu Y, Zhang Q, Friesner I, Jee HJ, Chen ZS, and Wang J (2021). Disrupted population coding in the prefrontal cortex underlies pain aversion. Cell Rep 37, 109978. 10.1016/j.celrep.2021.109978. [PubMed: 34758316]
10. Ji G, and Neugebauer V (2011). Pain-related deactivation of medial prefrontal cortical neurons involves mGluR1 and GABA(A) receptors. J Neurophysiol 106, 2642–2652. 10.1152/jn.00461.2011. [PubMed: 21880942]
11. Kelly CJ, Huang M, Meltzer H, and Martina M (2016). Reduced Glutamatergic Currents and Dendritic Branching of Layer 5 Pyramidal Cells Contribute to Medial Prefrontal Cortex Deactivation in a Rat Model of Neuropathic Pain. Front Cell Neurosci 10, 133. 10.3389/fncel.2016.00133. [PubMed: 27252623]
12. Radzicki D, Pollema-Mays SL, Sanz-Clemente A, and Martina M (2017). Loss of M1 Receptor Dependent Cholinergic Excitation Contributes to mPFC Deactivation in Neuropathic Pain. J Neurosci 37, 2292–2304. 10.1523/JNEUROSCI.1553-16.2017. [PubMed: 28137966]
13. Cheriyan J, and Sheets PL (2018). Altered Excitability and Local Connectivity of mPFC-PAG Neurons in a Mouse Model of Neuropathic Pain. J Neurosci 38, 4829–4839. 10.1523/JNEUROSCI.2731-17.2018. [PubMed: 29695413]
14. Huang J, Gadotti VM, Chen L, Souza IA, Huang S, Wang D, Ramakrishnan C, Deisseroth K, Zhang Z, and Zamponi GW (2019). A neuronal circuit for activating descending modulation of neuropathic pain. Nat Neurosci 22, 1659–1668. 10.1038/s41593-019-0481-5. [PubMed: 31501573]
15. Ji G, and Neugebauer V (2014). CB1 augments mGluR5 function in medial prefrontal cortical neurons to inhibit amygdala hyperactivity in an arthritis pain model. Eur J Neurosci 39, 455–466. 10.1111/ejn.12432. [PubMed: 24494685]
16. Zhou H, Martinez E, Lin HH, Yang R, Dale JA, Liu K, Huang D, and Wang J (2018). Inhibition of the Prefrontal Projection to the Nucleus Accumbens Enhances Pain Sensitivity and Affect. Front Cell Neurosci 12, 240. 10.3389/fncel.2018.00240. [PubMed: 30150924]
17. Gimpl G, and Fahrenholz F (2001). The oxytocin receptor system: structure, function, and regulation. Physiol Rev 81, 629–683. 10.1152/physrev.2001.81.2.629. [PubMed: 11274341]
18. Marlin BJ, Mitre M, D'Amour J A, Chao MV, and Froemke RC (2015). Oxytocin enables maternal behaviour by balancing cortical inhibition. Nature 520, 499–504. 10.1038/nature14402. [PubMed: 25874674]
19. Nishimori K, Young LJ, Guo Q, Wang Z, Insel TR, and Matzuk MM (1996). Oxytocin is required for nursing but is not essential for parturition or reproductive behavior. Proc Natl Acad Sci U S A 93, 11699–11704. 10.1073/pnas.93.21.11699. [PubMed: 8876199]

20. Pedersen CA, and Prange AJ Jr. (1979). Induction of maternal behavior in virgin rats after intracerebroventricular administration of oxytocin. Proc Natl Acad Sci U S A 76, 6661–6665. 10.1073/pnas.76.12.6661. [PubMed: 293752]
21. Hasan MT, Althammer F, Silva da Gouveia M, Goyon S, Eliava M, Lefevre A, Kerspern D, Schimmer J, Raftogianni A, Wahis J, et al. (2019). A Fear Memory Engram and Its Plasticity in the Hypothalamic Oxytocin System. Neuron 103, 133–146 e138. 10.1016/j.neuron.2019.04.029. [PubMed: 31104950]
22. Knobloch HS, Charlet A, Hoffmann LC, Eliava M, Khrulev S, Cetin AH, Osten P, Schwarz MK, Seeburg PH, Stoop R, and Grinevich V (2012). Evoked axonal oxytocin release in the central amygdala attenuates fear response. Neuron 73, 553–566. 10.1016/j.neuron.2011.11.030. [PubMed: 22325206]
23. Neumann ID, and Landgraf R (2012). Balance of brain oxytocin and vasopressin: implications for anxiety, depression, and social behaviors. Trends Neurosci 35, 649–659. 10.1016/j.tins.2012.08.004. [PubMed: 22974560]
24. Landgraf R, and Neumann ID (2004). Vasopressin and oxytocin release within the brain: a dynamic concept of multiple and variable modes of neuropeptide communication. Front Neuroendocrinol 25, 150–176. 10.1016/j.yfrne.2004.05.001. [PubMed: 15589267]
25. Sofroniew MV (1983). Morphology of vasopressin and oxytocin neurones and their central and vascular projections. Prog Brain Res 60, 101–114. 10.1016/S0079-6123(08)64378-2. [PubMed: 6198686]
26. Swanson LW, and Sawchenko PE (1983). Hypothalamic integration: organization of the paraventricular and supraoptic nuclei. Annu Rev Neurosci 6, 269–324. 10.1146/annurev.ne.06.030183.001413. [PubMed: 6132586]
27. Grinevich V, Knobloch-Bollmann HS, Eliava M, Busnelli M, and Chini B (2016). Assembling the Puzzle: Pathways of Oxytocin Signaling in the Brain. Biol Psychiatry 79, 155–164. 10.1016/j.biopsych.2015.04.013. [PubMed: 26001309]
28. Nakajima M, Gorlich A, and Heintz N (2014). Oxytocin modulates female sociosexual behavior through a specific class of prefrontal cortical interneurons. Cell 159, 295–305. 10.1016/j.cell.2014.09.020. [PubMed: 25303526]
29. Eliava M, Melchior M, Knobloch-Bollmann HS, Wahis J, da Silva Gouveia M, Tang Y, Ciobanu AC, Triana Del Rio R, Roth LC, Althammer F, et al. (2016). A New Population of Parvocellular Oxytocin Neurons Controlling Magnocellular Neuron Activity and Inflammatory Pain Processing. Neuron 89, 1291–1304. 10.1016/j.neuron.2016.01.041. [PubMed: 26948889]
30. Jo YH, Stoeckel ME, Freund-Mercier MJ, and Schlichter R (1998). Oxytocin modulates glutamatergic synaptic transmission between cultured neonatal spinal cord dorsal horn neurons. J Neurosci 18, 2377–2386. 10.1523/JNEUROSCI.18-07-02377.1998. [PubMed: 9502799]
31. Juif PE, Breton JD, Rajalu M, Charlet A, Goumon Y, and Poisbeau P (2013). Long-lasting spinal oxytocin analgesia is ensured by the stimulation of allopregnanolone synthesis which potentiates GABA(A) receptor-mediated synaptic inhibition. J Neurosci 33, 16617–16626. 10.1523/JNEUROSCI.3084-12.2013. [PubMed: 24133265]
32. Schoenen J, Lotstra F, Vierendeels G, Reznik M, and Vanderhaeghen JJ (1985). Substance P, enkephalins, somatostatin, cholecystokinin, oxytocin, and vasopressin in human spinal cord. Neurology 35, 881–890. 10.1212/wnl.35.6.881. [PubMed: 2582309]
33. Swanson LW, and McKellar S (1979). The distribution of oxytocin- and neurophysin-stained fibers in the spinal cord of the rat and monkey. J Comp Neurol 188, 87–106. 10.1002/cne.901880108. [PubMed: 115910]
34. Condes-Lara M, Martinez-Lorenzana G, Rubio-Beltran E, Rodriguez-Jimenez J, Rojas-Piloni G, and Gonzalez-Hernandez A (2015). Hypothalamic paraventricular nucleus stimulation enhances c-Fos expression in spinal and supraspinal structures related to pain modulation. Neurosci Res 98, 59–63. 10.1016/j.neures.2015.04.004. [PubMed: 25933550]
35. Huber D, Veinante P, and Stoop R (2005). Vasopressin and oxytocin excite distinct neuronal populations in the central amygdala. Science 308, 245–248. 10.1126/science.1105636. [PubMed: 15821089]

36. Yang J, Li P, Liang JY, Pan YJ, Yan XQ, Yan FL, Hao F, Zhang XY, Zhang J, Qiu PY, and Wang DX (2011). Oxytocin in the periaqueductal grey regulates nociception in the rat. Regul Pept 169, 39–42. 10.1016/j.regpep.2011.04.007. [PubMed: 21545817]
37. Campbell P, Ophir AG, and Phelps SM (2009). Central vasopressin and oxytocin receptor distributions in two species of singing mice. J Comp Neurol 516, 321–333. 10.1002/cne.22116. [PubMed: 19637308]
38. Vargas-Martinez F, Uvnas-Moberg K, Petersson M, Olausson HA, and Jimenez-Estrada I (2014). Neuropeptides as neuroprotective agents: Oxytocin a forefront developmental player in the mammalian brain. Prog Neurobiol 123, 37–78. 10.1016/j.pneurobio.2014.10.001. [PubMed: 25449701]
39. Boll S, Almeida de Minas AC, Raftogianni A, Herpertz SC, and Grinevich V (2018). Oxytocin and Pain Perception: From Animal Models to Human Research. Neuroscience 387, 149–161. 10.1016/j.neuroscience.2017.09.041. [PubMed: 28965836]
40. Singh A, Patel D, Li A, Hu L, Zhang Q, Liu Y, Guo X, Robinson E, Martinez E, Doan L, et al. (2020). Mapping Cortical Integration of Sensory and Affective Pain Pathways. Curr Biol 30, 1703–1715 e1705. 10.1016/j.cub.2020.02.091. [PubMed: 32220320]
41. Zhang Q, Manders T, Tong AP, Yang R, Garg A, Martinez E, Zhou H, Dale J, Goyal A, Urien L, et al. (2017). Chronic pain induces generalized enhancement of aversion. eLife 6, e25302. 10.7554/eLife.25302. [PubMed: 28524819]
42. Johansen JP, Fields HL, and Manning BH (2001). The affective component of pain in rodents: direct evidence for a contribution of the anterior cingulate cortex. Proc Natl Acad Sci U S A 98, 8077–8082. 10.1073/pnas.141218998. [PubMed: 11416168]
43. King T, Vera-Portocarrero L, Gutierrez T, Vanderah TW, Dussor G, Lai J, Fields HL, and Porreca F (2009). Unmasking the tonic-aversive state in neuropathic pain. Nat Neurosci 12, 1364–1366. 10.1038/nn.2407. [PubMed: 19783992]
44. Zhang Q, Hu S, Talay R, Xiao Z, Rosenberg D, Liu Y, Sun G, Li A, Caravan B, Singh A, et al. (2021). A prototype closed-loop brain-machine interface for the study and treatment of pain. Nat Biomed Eng 10.1038/s41551-021-00736-7.
45. Elands J, Barberis C, Jard S, Tribollet E, Dreifuss JJ, Bankowski K, Manning M, and Sawyer WH (1988). 125I-labelled d(CH2)5[Tyr(Me)2,Thr4,Tyr-NH2(9)]OVT: a selective oxytocin receptor ligand. Eur J Pharmacol 147, 197–207. 10.1016/0014-2999(88)90778-9. [PubMed: 2835249]
46. Grazzini E, Guillon G, Mouillac B, and Zingg HH (1998). Inhibition of oxytocin receptor function by direct binding of progesterone. Nature 392, 509–512. 10.1038/33176. [PubMed: 9548257]
47. Friedrich J, Zhou P, and Paninski L (2017). Fast online deconvolution of calcium imaging data. PLoS Comput Biol 13, e1005423. 10.1371/journal.pcbi.1005423. [PubMed: 28291787]
48. De Vico Fallani F, Richiardi J, Chavez M, and Achard S (2014). Graph analysis of functional brain networks: practical issues in translational neuroscience. Philos Trans R Soc Lond B Biol Sci 369. 10.1098/rstb.2013.0521.
49. Kwon H, Choi YH, and Lee JM (2019). A Physarum Centrality Measure of the Human Brain Network. Sci Rep 9, 5907. 10.1038/s41598-019-42322-7. [PubMed: 30976010]
50. Sun G, Zeng F, McCartin M, Zhang Q, Xu H, Liu Y, Chen ZS, and Wang J (2022). Closed-loop stimulation using a multiregion brain-machine interface has analgesic effects in rodents. Sci Transl Med 14, eabm5868. 10.1126/scitranslmed.abm5868. [PubMed: 35767651]
51. Basbaum AI, and Fields HL (1984). Endogenous pain control systems: brainstem spinal pathways and endorphin circuitry. Annu Rev Neurosci 7, 309–338. 10.1146/annurev.ne.07.030184.001521. [PubMed: 6143527]
52. Motojima Y, Matsuura T, Yoshimura M, Hashimoto H, Saito R, Ueno H, Maruyama T, Sonoda S, Suzuki H, Kawasaki M, et al. (2017). Comparison of the induction of c-fos-eGFP and Fos protein in the rat spinal cord and hypothalamus resulting from subcutaneous capsaicin or formalin injection. Neuroscience 356, 64–77. 10.1016/j.neuroscience.2017.05.015. [PubMed: 28527956]
53. Owen SF, Tuncdemir SN, Bader PL, Tirko NN, Fishell G, and Tsien RW (2013). Oxytocin enhances hippocampal spike transmission by modulating fast-spiking interneurons. Nature 500, 458–462. 10.1038/nature12330. [PubMed: 23913275]

54. Tirko NN, Eyring KW, Carcea I, Mitre M, Chao MV, Froemke RC, and Tsien RW (2018). Oxytocin Transforms Firing Mode of CA2 Hippocampal Neurons. Neuron 100, 593–608 e593. 10.1016/j.neuron.2018.09.008. [PubMed: 30293821]
55. Baliki MN, Petre B, Torbey S, Herrmann KM, Huang L, Schnitzer TJ, Fields HL, and Apkarian AV (2012). Corticostriatal functional connectivity predicts transition to chronic back pain. Nat Neurosci 15, 1117–1119. 10.1038/nn.3153. [PubMed: 22751038]
56. Kano M, Grinsvall C, Ran Q, Dupont P, Morishita J, Muratsubaki T, Mugikura S, Ly HG, Tornblom H, Ljungberg M, et al. (2020). Resting state functional connectivity of the pain matrix and default mode network in irritable bowel syndrome: a graph theoretical analysis. Sci Rep 10, 11015. 10.1038/s41598-020-67048-9. [PubMed: 32620938]
57. Mutso AA, Radzicki D, Baliki MN, Huang L, Banisadr G, Centeno MV, Radulovic J, Martina M, Miller RJ, and Apkarian AV (2012). Abnormalities in hippocampal functioning with persistent pain. J Neurosci 32, 5747–5756. 10.1523/JNEUROSCI.0587-12.2012. [PubMed: 22539837]
58. Spisak T, Kincses B, Schlitt F, Zunhammer M, Schmidt-Wilcke T, Kincses ZT, and Bingel U (2020). Pain-free resting-state functional brain connectivity predicts individual pain sensitivity. Nat Commun 11, 187. 10.1038/s41467-019-13785-z. [PubMed: 31924769]
59. Vachon-Presseau E, Berger SE, Abdullah TB, Griffith JW, Schnitzer TJ, and Apkarian AV (2019). Identification of traits and functional connectivity-based neurotraits of chronic pain. PLoS Biol 17, e3000349. 10.1371/journal.pbio.3000349. [PubMed: 31430270]
60. Bonifazi P, and Massobrio P (2019). Reconstruction of Functional Connectivity from Multielectrode Recordings and Calcium Imaging. Adv Neurobiol 22, 207–231. 10.1007/978-3-030-11135-9_9. [PubMed: 31073938]
61. Sporns O (2018). Graph theory methods: applications in brain networks. Dialogues Clin Neurosci 20, 111–121. 10.31887/DCNS.2018.20.2/osporns. [PubMed: 30250388]
62. Bilbao A, Falfan-Melgoza C, Leixner S, Becker R, Singaravelu SK, Sack M, Sartorius A, Spanagel R, and Weber-Fahr W (2018). Longitudinal Structural and Functional Brain Network Alterations in a Mouse Model of Neuropathic Pain. Neuroscience 387, 104–115. 10.1016/j.neuroscience.2018.04.020. [PubMed: 29694917]
63. Komaki Y, Hikishima K, Shibata S, Konomi T, Seki F, Yamada M, Miyasaka N, Fujiyoshi K, Okano HJ, Nakamura M, and Okano H (2016). Functional brain mapping using specific sensory-circuit stimulation and a theoretical graph network analysis in mice with neuropathic allodynia. Sci Rep 6, 37802. 10.1038/srep37802. [PubMed: 27898057]
64. Minati L, Varotto G, D'Incerti L, Panzica F, and Chan D (2013). From brain topography to brain topology: relevance of graph theory to functional neuroscience. Neuroreport 24, 536–543. 10.1097/WNR.0b013e3283621234. [PubMed: 23660679]
65. Redcay E, Moran JM, Mavros PL, Tager-Flusberg H, Gabrieli JD, and Whitfield-Gabrieli S (2013). Intrinsic functional network organization in high-functioning adolescents with autism spectrum disorder. Front Hum Neurosci 7, 573. 10.3389/fnhum.2013.00573. [PubMed: 24062673]
66. Kobak D, Brendel W, Constantinidis C, Feierstein CE, Kepecs A, Mainen ZF, Qi XL, Romo R, Uchida N, and Machens CK (2016). Demixed principal component analysis of neural population data. eLife 5, e10989. 10.7554/eLife.10989. [PubMed: 27067378]
67. Markowitz DA, Curtis CE, and Pesaran B (2015). Multiple component networks support working memory in prefrontal cortex. Proc Natl Acad Sci U S A 112, 11084–11089. 10.1073/pnas.1504172112. [PubMed: 26283366]
68. Murray JD, Bernacchia A, Roy NA, Constantinidis C, Romo R, and Wang XJ (2017). Stable population coding for working memory coexists with heterogeneous neural dynamics in prefrontal cortex. Proc Natl Acad Sci U S A 114, 394–399. 10.1073/pnas.1619449114. [PubMed: 28028221]
69. Dabrowska J, Hazra R, Ahern TH, Guo JD, McDonald AJ, Mascagni F, Muller JF, Young LJ, and Rainnie DG (2011). Neuroanatomical evidence for reciprocal regulation of the corticotrophin-releasing factor and oxytocin systems in the hypothalamus and the bed nucleus of the stria terminalis of the rat: Implications for balancing stress and affect. Psychoneuroendocrinology 36, 1312–1326. 10.1016/j.psyneuen.2011.03.003. [PubMed: 21481539]

70. Ebner K, Bosch OJ, Kromer SA, Singewald N, and Neumann ID (2005). Release of oxytocin in the rat central amygdala modulates stress-coping behavior and the release of excitatory amino acids. Neuropsychopharmacology 30, 223–230. 10.1038/sj.npp.1300607. [PubMed: 15536493]
71. Grund T, Goyon S, Li Y, Eliava M, Liu H, Charlet A, Grinevich V, and Neumann ID (2017). Neuropeptide S Activates Paraventricular Oxytocin Neurons to Induce Anxiolysis. J Neurosci 37, 12214–12225. 10.1523/JNEUROSCI.2161-17.2017. [PubMed: 29118105]
72. Neumann ID, and Slattery DA (2016). Oxytocin in General Anxiety and Social Fear: A Translational Approach. Biol Psychiatry 79, 213–221. 10.1016/j.biopsych.2015.06.004. [PubMed: 26208744]
73. Vacher CM, Fretier P, Creminon C, Calas A, and Hardin-Pouzet H (2002). Activation by serotonin and noradrenaline of vasopressin and oxytocin expression in the mouse paraventricular and supraoptic nuclei. J Neurosci 22, 1513–1522. 10.1523/JNEUROSCI.22-05-01513.2002. [PubMed: 11880481]
74. Wotjak CT, Ganster J, Kohl G, Holsboer F, Landgraf R, and Engelmann M (1998). Dissociated central and peripheral release of vasopressin, but not oxytocin, in response to repeated swim stress: new insights into the secretory capacities of peptidergic neurons. Neuroscience 85, 1209–1222. 10.1016/s0306-4522(97)00683-0. [PubMed: 9681958]
75. Ji G, Sun H, Fu Y, Li Z, Pais-Vieira M, Galhardo V, and Neugebauer V (2010). Cognitive impairment in pain through amygdala-driven prefrontal cortical deactivation. J Neurosci 30, 5451–5464. 10.1523/JNEUROSCI.0225-10.2010. [PubMed: 20392966]
76. Wang GQ, Cen C, Li C, Cao S, Wang N, Zhou Z, Liu XM, Xu Y, Tian NX, Zhang Y, et al. (2015). Deactivation of excitatory neurons in the prelimbic cortex via Cdk5 promotes pain sensation and anxiety. Nat Commun 6, 7660. 10.1038/ncomms8660. [PubMed: 26179626]
77. Sabihi S, Durosko NE, Dong SM, and Leuner B (2014). Oxytocin in the prelimbic medial prefrontal cortex reduces anxiety-like behavior in female and male rats. Psychoneuroendocrinology 45, 31–42. 10.1016/j.psyneuen.2014.03.009. [PubMed: 24845174]
78. Tapp DN, Singstock MD, Gottliebson MS, and McMurray MS (2020). Central but not peripheral oxytocin administration reduces risk-based decision-making in male rats. Horm Behav 125, 104840. 10.1016/j.yhbeh.2020.104840. [PubMed: 32795469]
79. Pnevmatikakis EA, Soudry D, Gao Y, Machado TA, Merel J, Pfau D, Reardon T, Mu Y, Lacefield C, Yang W, et al. (2016). Simultaneous Denoising, Deconvolution, and Demixing of Calcium Imaging Data. Neuron 89, 285–299. 10.1016/j.neuron.2015.11.037. [PubMed: 26774160]
80. Vander Weele CM, Siciliano CA, Matthews GA, Namburi P, Izadmehr EM, Espinel IC, Nieh EH, Schut EHS, Padilla-Coreano N, Burgos-Robles A, et al. (2018). Dopamine enhances signal-to-noise ratio in cortical-brainstem encoding of aversive stimuli. Nature 563, 397–401. 10.1038/s41586-018-0682-1. [PubMed: 30405240]
81. Zhou P, Resendez SL, Rodriguez-Romaguera J, Jimenez JC, Neufeld SQ, Giovannucci A, Friedrich J, Pnevmatikakis EA, Stuber GD, Hen R, et al. (2018). Efficient and accurate extraction of in vivo calcium signals from microendoscopic video data. eLife 7, e28728. 10.7554/eLife.28728. [PubMed: 29469809]
82. Sheintuch L, Rubin A, Brande-Eilat N, Geva N, Sadeh N, Pinchasof O, and Ziv Y (2017). Tracking the Same Neurons across Multiple Days in Ca(2+) Imaging Data. Cell Rep 21, 1102–1115. 10.1016/j.celrep.2017.10.013. [PubMed: 29069591]
83. Goffer Y, Xu D, Eberle SE, D'Amour J, Lee M, Tukey D, Froemke RC, Ziff EB, and Wang J (2013). Calcium-permeable AMPA receptors in the nucleus accumbens regulate depression-like behaviors in the chronic neuropathic pain state. J Neurosci 33, 19034–19044. 10.1523/JNEUROSCI.2454-13.2013. [PubMed: 24285907]
84. Wang J, Goffer Y, Xu D, Tukey DS, Shamir DB, Eberle SE, Zou AH, Blanck TJ, and Ziff EB (2011). A single subanesthetic dose of ketamine relieves depression-like behaviors induced by neuropathic pain in rats. Anesthesiology 115, 812–821. 10.1097/ALN.0b013e31822f16ae. [PubMed: 21934410]
85. Hargreaves K, Dubner R, Brown F, Flores C, and Joris J (1988). A new and sensitive method for measuring thermal nociception in cutaneous hyperalgesia. Pain 32, 77–88. 10.1016/0304-3959(88)90026-7. [PubMed: 3340425]

86. Corder G, Ahanonu B, Grewe BF, Wang D, Schnitzer MJ, and Scherrer G (2019). An amygdalar neural ensemble that encodes the unpleasantness of pain. Science 363, 276–281. 10.1126/science.aap8586. [PubMed: 30655440]

Highlights

- Oxytocin enhances population nociceptive activity in the PL-PFC in rats
- Oxytocin released from PVN alters the excitation-inhibition balance in the PL-PFC
- The oxytocinergic PVN-PFC projection regulates acute and chronic pain

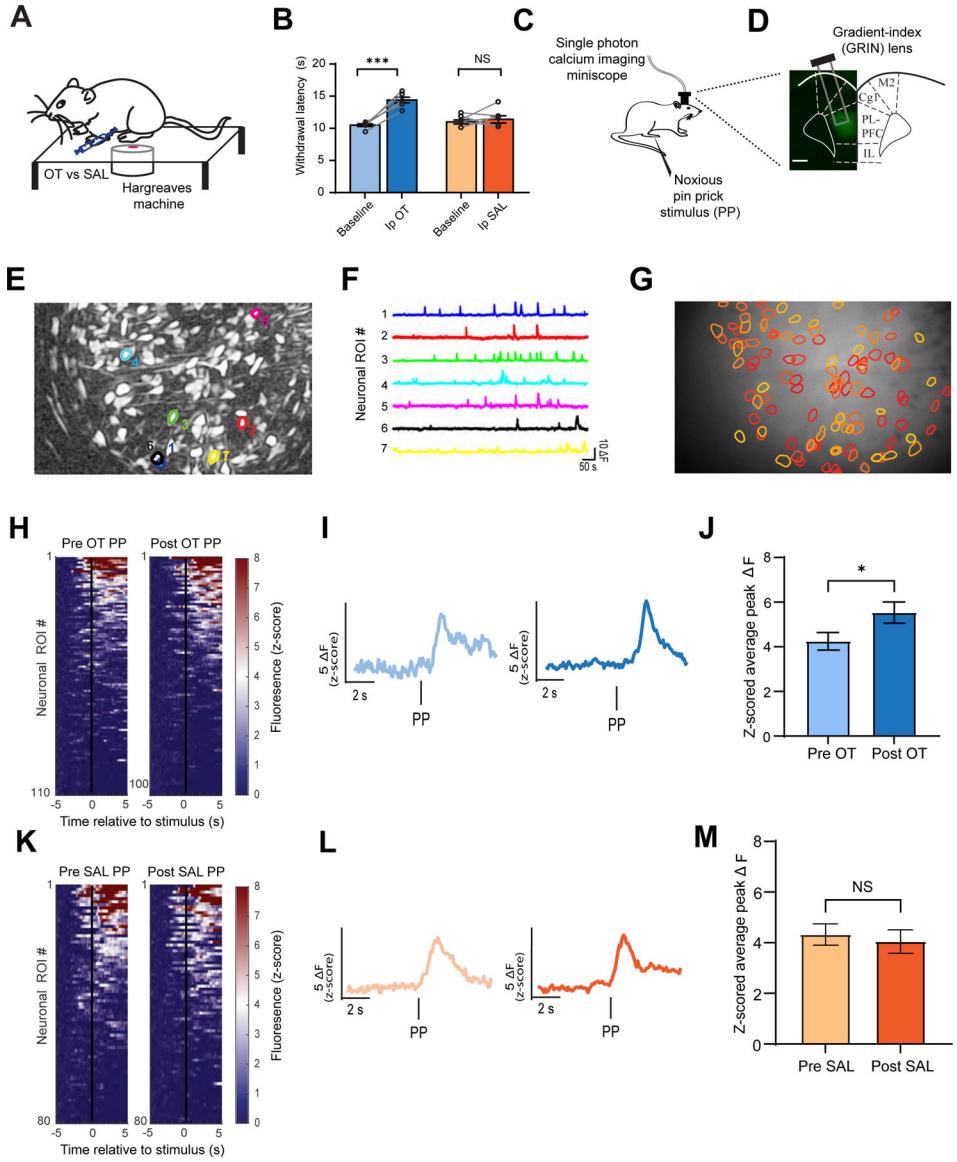

Figure 1. Oxytocin increases population nociceptive response in the PL-PFC.

(A) Hargreaves test on a rat injected intraperitoneally (Ip) with oxytocin (OT) or saline (SAL).

(B) Oxytocin prolonged the withdrawal latency. (paired t test; OT versus Baseline: ***$p < 0.001$; SAL vs Baseline: $p = 0.5769$; $n = 6$ animals).

(C) Schematic of calcium imaging experiments.

(D) Gradient-index (GRIN) lens placement and GCaMP6f expression in the PL-PFC.

(E) Field of view and sample identified contours of neuronal regions of interest (ROIs).

(F) Calcium activity of identified ROI traces.

(G) Map of PL-PFC ROIs with contours overlaid on imaging field of view.

(H) Mean Ca^{2+} response (z-scored) across all trials for all ROIs before and after OT. Neuronal activity is ordered from high to low responses after acute noxious pin prick (PP) stimulus. ($n = 110$ pre-OT, 104 post-OT ROIs).

(I) Representative trace of pain-responsive neuronal ROI in response to PP before (light blue) and after (blue) OT administration.
(J) Pain-responsive ROIs in the PL-PFC exhibit increased activity after OT (*$p < 0.05$, unpaired t test; n = 99 pre-OT, 97 post-OT ROIs).
(K) Same as (H), but before and after SAL (n = 80 pre-SAL, 84 post-SAL ROIs).
(L) Same as (I), but before (light orange) and after (orange) SAL.
(M) Pain-responsive ROIs in the PL-PFC displayed no change in activity after SAL. ($p = 0.6596$, unpaired t test; n = 100 pre-SAL, 82 post-SAL ROIs).
Data are represented as mean ± S.E.M. See also Figure S1, S2.

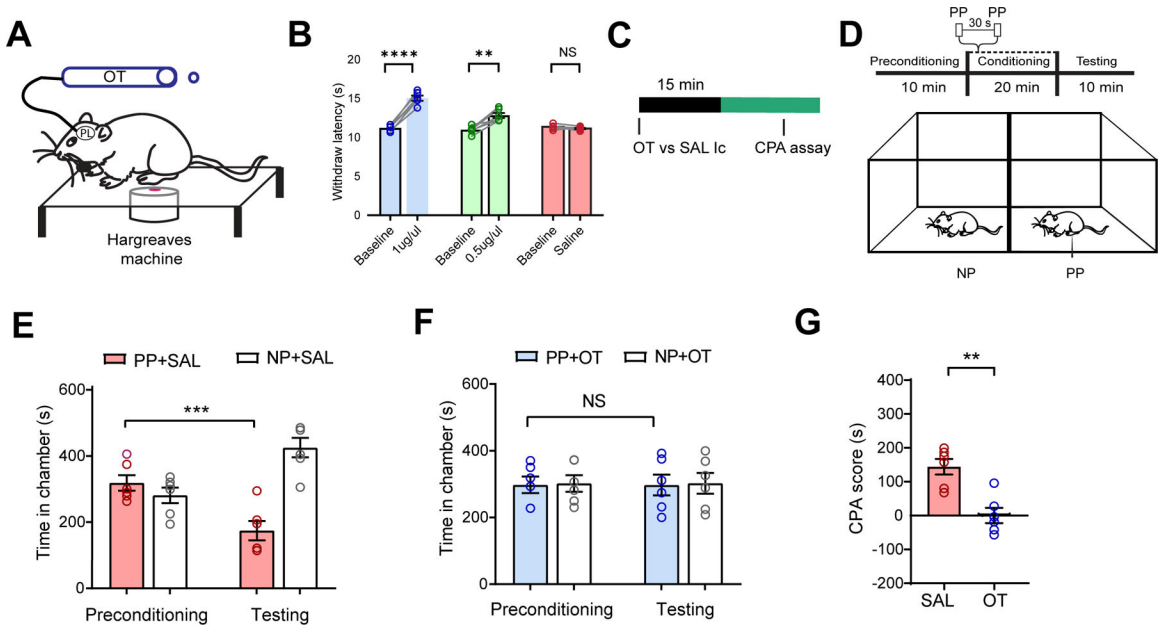

Figure 2. Oxytocin in the PL-PFC produces anti-nociceptive effects.

(A) Hargreaves test with OT delivered intracranially (Ic) to the PL-PFC.

(B) Intracranial OT at 0.5 μg and 1 μg increased withdrawal latency, compared with SAL (paired t test; 1 μg OT versus baseline: ****$p < 0.0001$; 0.5 μg OT versus baseline: **$p < 0.01$, SAL versus Baseline: $p = 0.2255$; $n = 6$ animals).

(C) Experimental timeline.

(D) Schematic of the CPA assay, where no noxious stimulus (no prick, NP) was paired with one chamber, and noxious PP was paired with the other chamber.

(E) Rats after SAL exhibited aversion to the chamber associated with PP (***$p < 0.001$, two-way ANOVA with repeated measures and Sidak's multiple comparisons test; $n = 6$ animals).

(F) Rats after OT exhibited no aversion to PP ($p = 0.9998$, same test as F, $n = 6$ animals).

(G) OT decreased aversion to PP in naïve rats (**$p < 0.01$, paired t test; $n = 6$ SAL and OT animals). Data are represented as mean ± S.E.M. See also Figure S3.

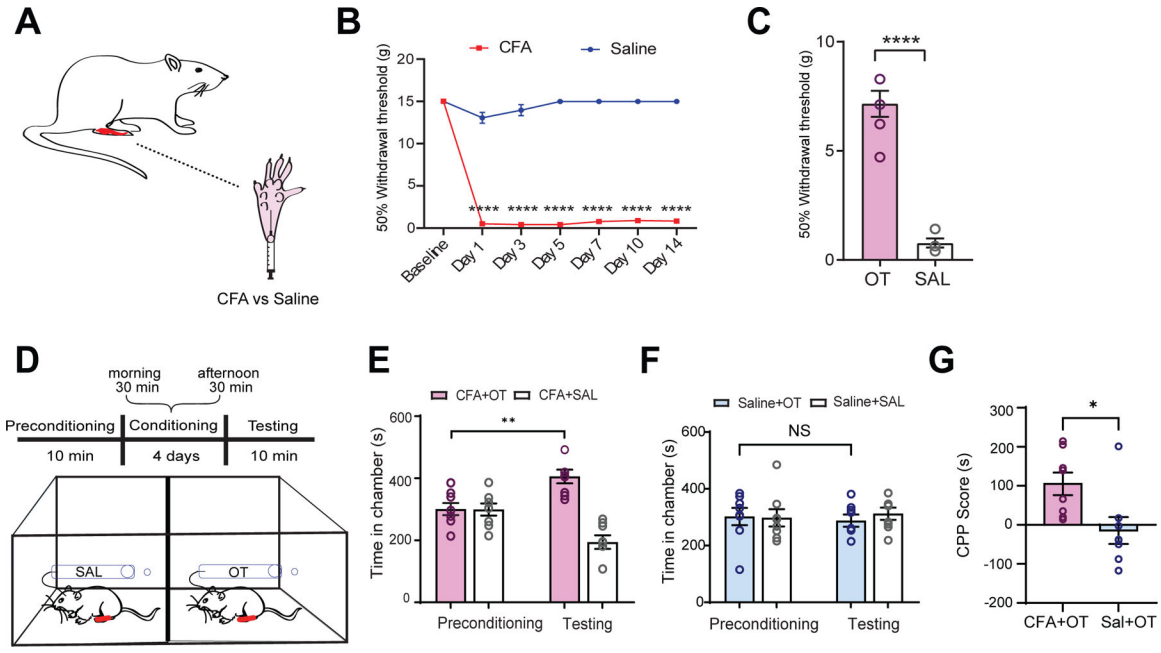

Figure 3. Oxytocin in the PL-PFC reduces chronic inflammatory pain

(A) Complete Freund's adjuvant (CFA) or saline injection to rat's hind paw.

(B) CFA decreased withdrawal threshold (****$p < 0.0001$, two-way ANOVA with repeated measures and Sidak's multiple comparisons test; n = 6 animals).

(C) Intracranial OT, compared SAL, increased the withdrawal threshold in CFA-treated rats (****$p < 0.0001$, unpaired t test; n = 6 animals).

(D) Conditioned place preference (CPP) assay on tonic pain in CFA rats. Rats had SAL delivered intracranially in one chamber and OT delivered in the opposite chamber.

(E) CFA-treated rats demonstrated a preference for the chamber associated with OT (**$p < 0.01$, n = 8 animals).

(F) Control rats that received subcutaneous saline injections to paw demonstrated no preference for OT treatment ($p = 0.8976$, n = 8 animals).

(G) CFA-treated rats exhibited a preference for the chamber associated with OT (*$p < 0.05$, unpaired t test; n = 8 CFA and saline animals).

Data are represented as mean ± S.E.M.

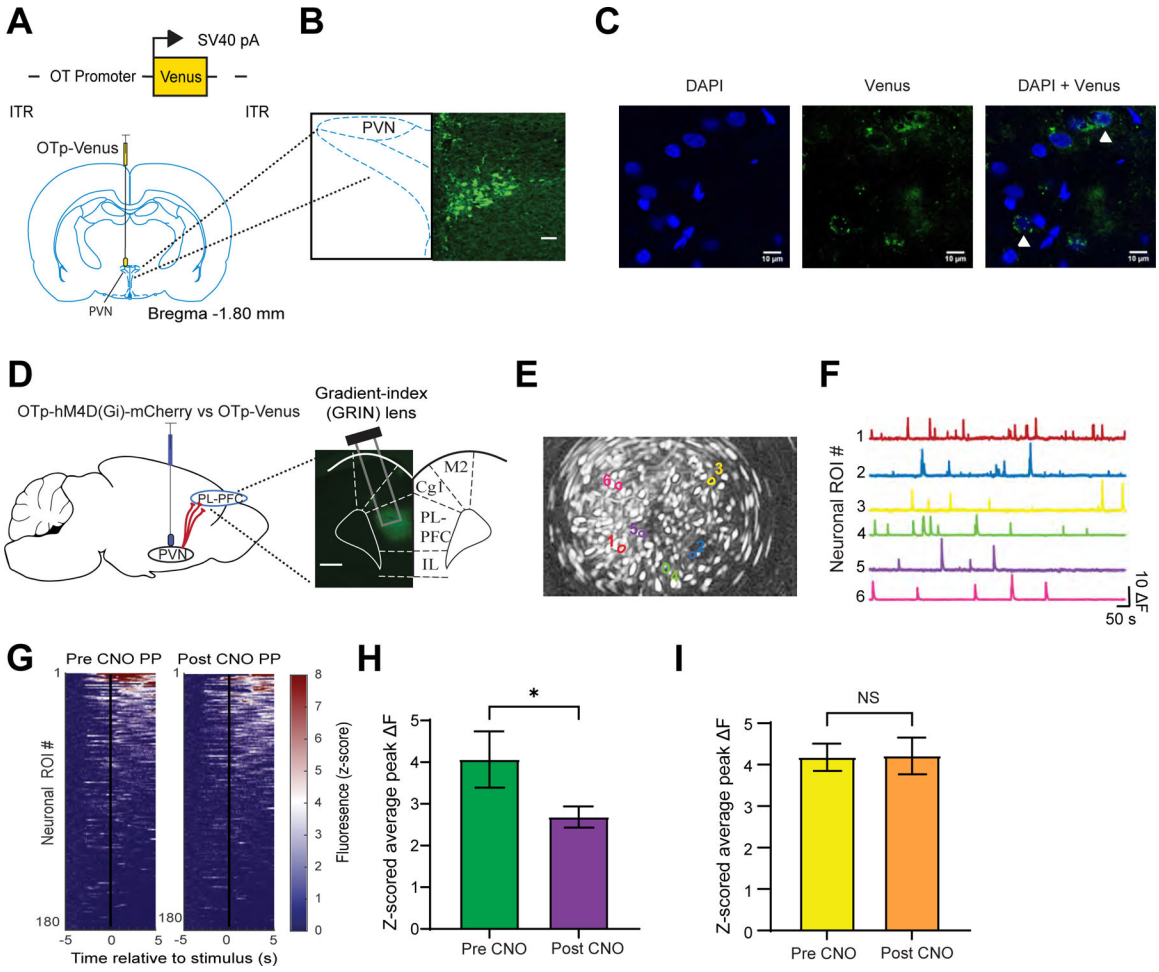

Figure 4. Chemogenetic inhibition of the PVN reduces the nociceptive response in PL-PFC

(A) Viral vector and injection site of OTp-Venus in the PVN.

(B) Fluorescence imaging of PVN neurons.

(C) High-magnitude fluorescence imaging of PVN axons (white triangle) in the PL-PFC.

(D) OTp-hM4D(Gi)-mCherry or OTp-Venus virus injection in the PVN and Gradient-index (GRIN) lens placement and GCaMP6f expression in the PL-PFC.

(E) Field of view and map of example PL-PFC ROIs.

(F) Representative Ca^{2+} activity traces of ROIs in E.

(G) Mean Ca^{2+} response for PL-PFC ROIs imaged in sessions before and after CNO, ranked from high to low Ca^{2+} responses after PP. (n = 187 pre-CNO, 193 post-CNO).

(H) Pain-responsive ROIs in rats injected with OTp-hM4D(Gi)-mCherry exhibited decreased Ca^{2+} activity after CNO (*$p < 0.05$, unpaired t test; n = 39 pre-CNO, 52 post-CNO).

(I) Pain-responsive ROIs in rats injected with OTp-Venus showed no changes in Ca^{2+} activity after CNO ($p = 0.9541$, n = 47 pre-CNO, 58 post-CNO).

Data are represented as mean ± S.E.M.

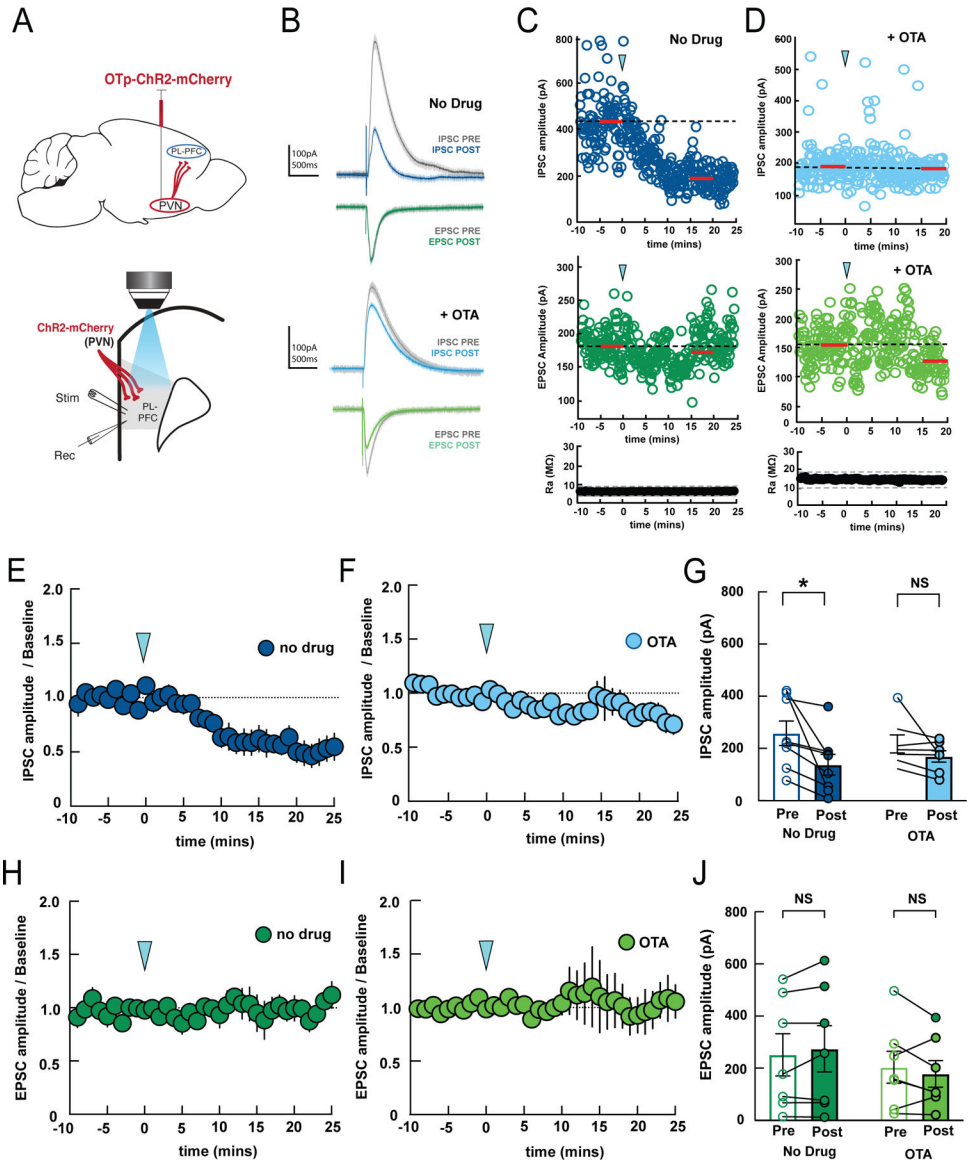

Figure 5. Optogenetic activation of the PVN axon terminals reduces synaptic inhibition in the PL-PFC

(A) Surgical (top) and recording (bottom) configurations. Blue light stimulation of ChR2-expressing PVN terminals in PL-PFC alters magnitude of post-synaptic currents evoked by local electrical stimulation (stim) recorded in whole-cell configuration (rec).

(B) Example IPSC and EPSC before (gray, baseline) and after optogenetic PVN stimulation (blue, IPSC 15–20 minutes post-stimulation; green, EPSC 15–20 minutes post-stimulation).

(C) Example recording showing time course of PVN stimulation (arrowhead) on IPSC amplitudes (top) and EPSC amplitudes (middle) from the same cell. Red bars, time windows for statistical analysis. Bottom, Ra was stable over the recording period; dashed lines, ±20% from average of baseline Ra.

(D) Example recording showing time course of PVN stimulation with 1 μM OTA in bath; IPSCs, EPSCs, Ra were unaffected. (E,F) Summary of time course of effects of PVN

stimulation (arrowhead) on IPSCs in ACSF (E, n=8 recordings) or 1 μM OTA (F, n=7 recordings) added to the bath.

(G) Mean IPSC amplitudes during 5-minute baseline (Pre) and 15–20 minutes after optogenetic stimulation (Post). IPSCs were reduced by PVN stimulation in ACSF ('No Drug', p = 0.0128, two-way ANOVA with Bonferroni's multiple comparisons correction, n=8 recordings), but blocking oxytocin receptors prevented this effect ('OTA', p=0.50, n=7 recordings). (H,I) Summary of time course of EPSCs after PVN stimulation in ACSF (left) or 1 μM OTA (right).

(J) Mean EPSC amplitudes before and after PVN stimulation; no effect in either ACSF (p=0.57) or 1 μM OTA (p=0.46). Same cells as in (G).

Data are represented as mean ± S.E.M.

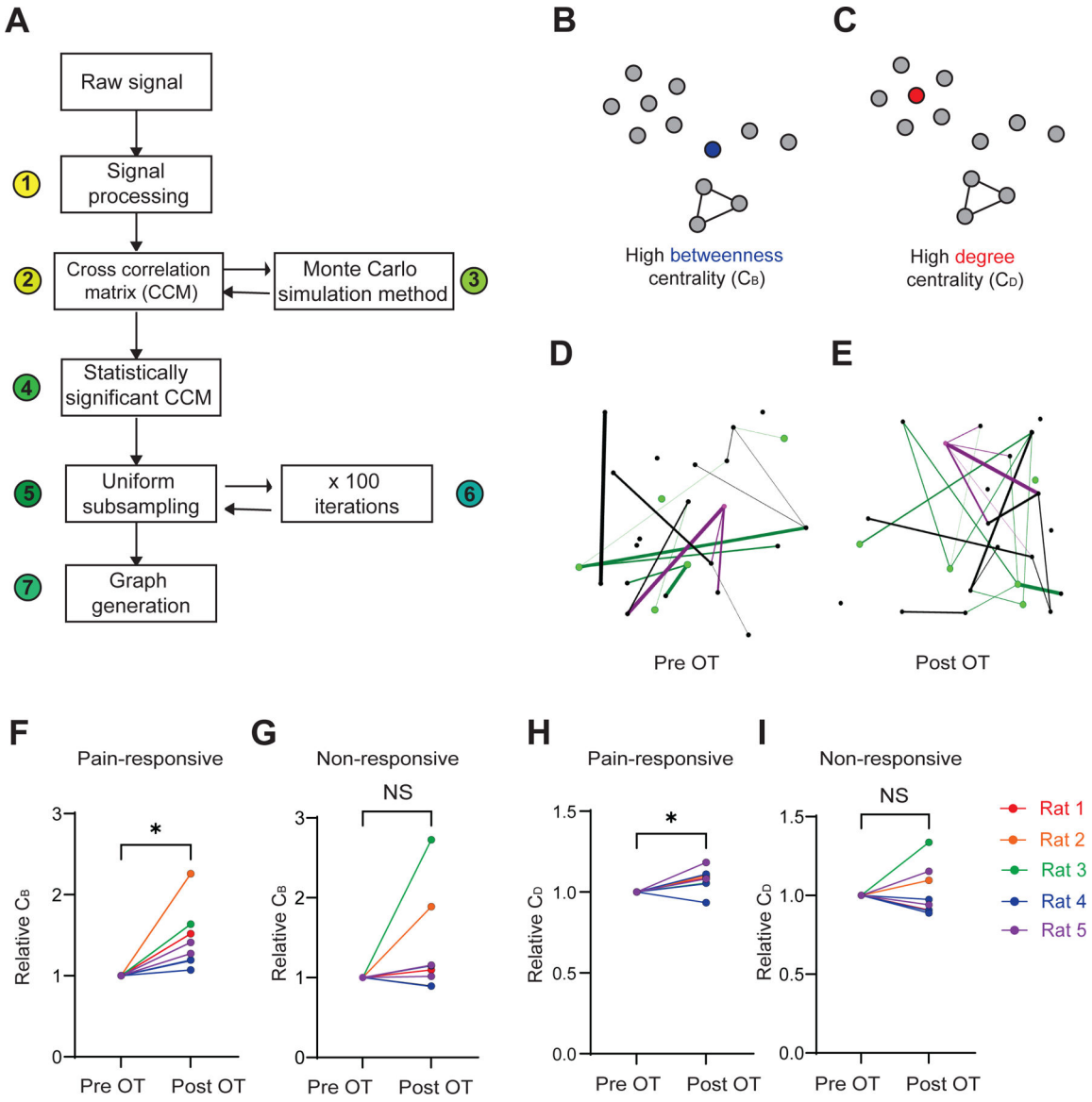

Figure 6. Oxytocin enhances functional connectivity in pain-responsive neurons

(A) Functional connectivity analysis. We processed the raw Ca^{2+} imaging signal by 1) Z-scored normalization and spike deconvolution; 2) a cross-correlation matrix generation using extracted spiking activity of ROIs; 3) Monte Carlo simulation method to create 4) a matrix of statistically significant correlations between neuronal ROIs; 5) uniform subsampling of pain-responsive and non-responsive ROIs were repeated 6) for 100 iterations; 7) graph generation for each iteration.

(B) Graph schematic demonstrating a node with high betweenness centrality (blue), as a central hub to multiple regions.

(C) Graph schematic exhibiting a node with high degree centrality (red), as it has the most connections to other nodes.

(D) An example graph from subsampled ROIs within the PL-PFC pre-OT. Green nodes: pain-responsive ROIs. Magenta nodes: ROI with the highest betweenness and degree centralities.

(E) Same as (D), but post-OT.

(F) Pain-responsive subpopulations demonstrated an increase in betweenness centrality (C_B) post-OT (*$p < 0.05$, paired t test).

(G) In non-responsive subpopulations, no significant change in C_B was observed post-OT ($p = 0.1634$).

(H) Pain-responsive subpopulations exhibited an increase in degree centrality (C_D) after OT administration (*$p < 0.05$).

(I) Non-responsive PL-PFC subpopulations did not exhibit a change in C_D post-OT ($p = 0.6738$).

Data are represented as mean ± S.E.M. n = 8 recordings from 5 rats. See also Figures S4, S5, and S6.

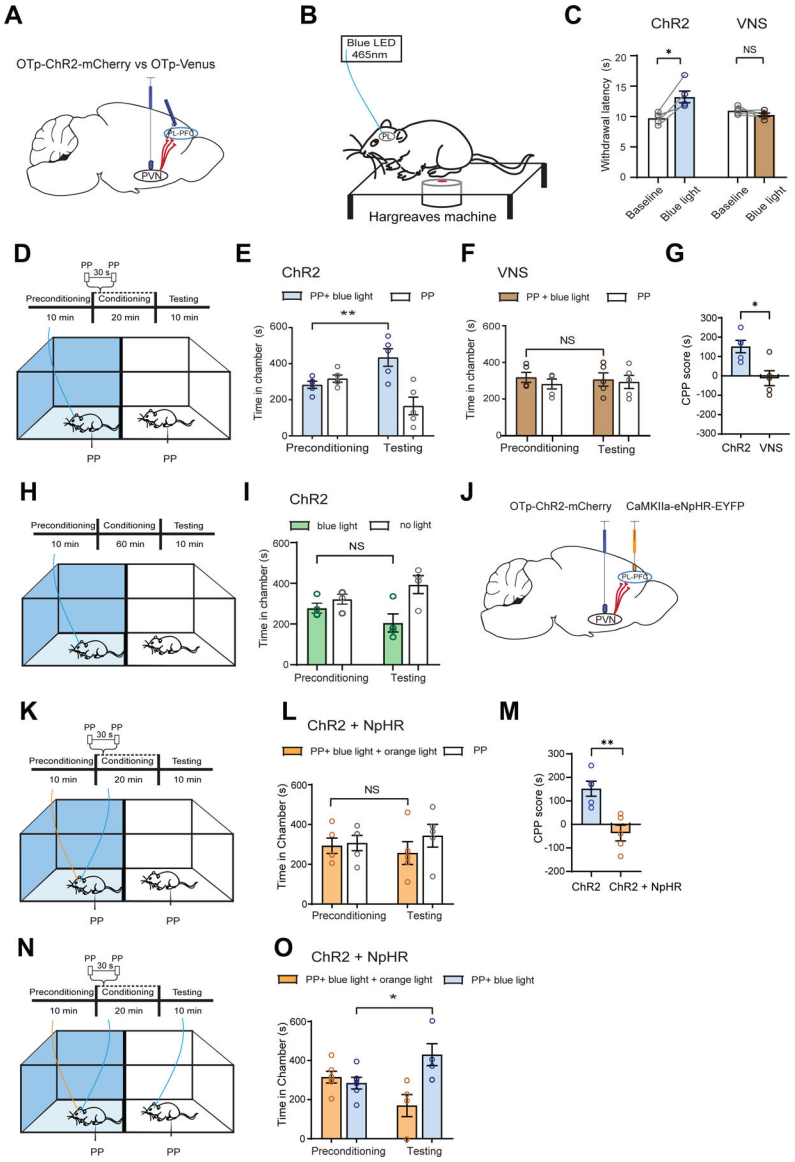

Figure 7. Direct projection from oxytocinergic neurons in the PVN to the PL-PFC regulates acute pain

(A) Injection of OTp-ChR2-mCherry or OTp-Venus into the PVN and insertion of optic fiber into the PL-PFC.

(B) Schematic of Hargreaves test.

(C) Light treatment of the PL-PFC prolonged withdrawal latency in ChR2 (blue) rats, compared with control VNS (brown) rats (paired t test; ChR2 versus baseline: *$p < 0.05$; VNS versus baseline: $p = 0.2170$; n = 5 ChR2 and VNS animals).

(D) CPP assay. One chamber received noxious PP paired with light treatment of the PL-PFC, and the other chamber received PP alone.

(E) ChR2 rats demonstrated increased preference for treatment chamber paired with light treatment of the PL-PFC (**$p < 0.01$, two-way ANOVA with repeated measures and Sidak's multiple comparisons test; n = 5 animals).

(F) VNS rats exhibited no change in preference for either chamber ($p = 0.9491$, $n = 5$ animals).
(G) ChR2 rats demonstrated preference for light treatment of the PL-PFC (*$p < 0.05$, unpaired t test; $n = 5$ ChR2 and $n = 5$ VNS animals).
(H) CPP assay in the absence of noxious stimuli. One chamber was paired with blue light stimulation of the PL-PFC; the other chamber was paired with no light.
(I) ChR2 rats demonstrated no preference for light treatment in the absence of noxious stimuli ($p = 0.4591$, $n = 4$ ChR2 animals).
(J) Injection of OTp-ChR2-mCherry into PVN and CamKIIa-eNpHR-EYFP into PL-PFC, with optic fibers implanted in both regions.
(K) CPP assay with PP. One chamber was paired with simultaneous blue light treatment of the PVN and orange light treatment of the PL-PFC; the other chamber was paired with no light treatment.
(L) Rats demonstrated no preference for the chamber paired with simultaneous PVN activation and PL-PFC inhibition ($p = 0.5215$, $n = 5$ animals).
(M) Rats preferred blue light activation of the PL-PFC relative to simultaneous activation of PVN and inhibition of PL-PFC (**$p < 0.01$, unpaired t test; $n = 5$ ChR2 and ChR2 + NpHR animals).
(N) CPP assay with PP. In rats with both ChR2 expression in the PVN and NpHR expression in the PL-PFC, one chamber was paired with simultaneous blue light treatment of the PVN and orange light treatment of the PL-PFC, while the other chamber was paired with only blue light stimulation of the PVN.
(O) Rats preferred the chamber associated with only blue light treatment of the PVN over chamber paired with simultaneous activation of PVN and inhibition of PL-PFC (*$p < 0.05$, $n = 6$ animals).
Data are represented as mean ± S.E.M.

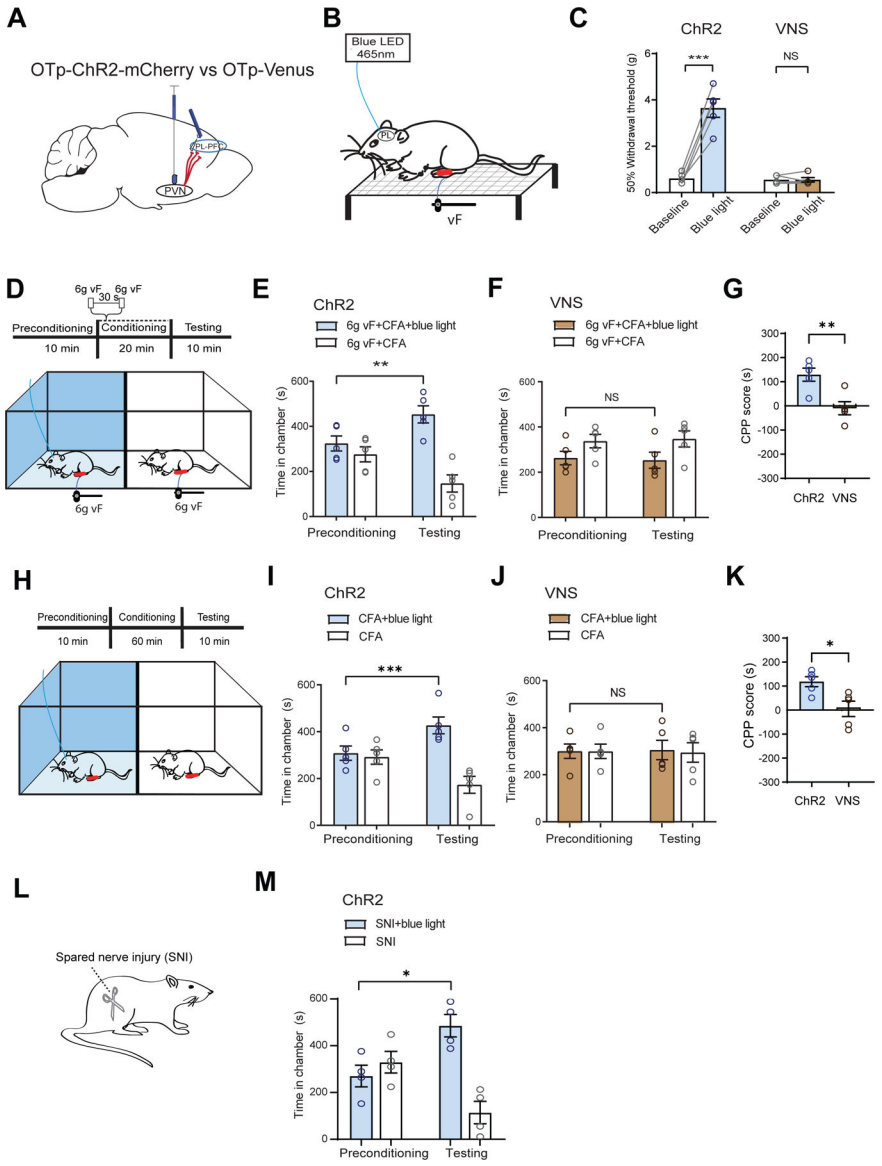

Figure 8. Activation of axon terminals of oxytocinergic neurons from the PVN in the PL-PFC inhibits chronic pain

(A) Injection of OTp-ChR2-mCherry or OTp-Venus into the PVN and optic fiber into the PL-PFC.

(B) Schematic of mechanical allodynia.

(C) Light treatment of the PL-PFC increased withdrawal threshold in CFA-treated ChR2 (blue) rats, compared with VNS (control) rats. (paired t test; ChR2 versus baseline: ***$p < 0.001$; VNS versus baseline; $p = 0.9911$; $n = 5$ ChR2 and VNS animals).

(D) CPP assay in CFA-treated rats. In one chamber, rats received noxious mechanical stimulus (6g vF) paired with light treatment of the PL-PFC. In the other chamber, rats received 6g vF alone.

(E) ChR2 rats showed preference for the chamber paired with light treatment (**$p < 0.01$, two-way ANOVA with repeated measures and Sidak's multiple comparisons test; $n = 5$ ChR2 animals).

(F) VNS rats showed no preference for either chamber ($p = 0.9242$, $n = 5$ VNS animals).
(G) ChR2 CFA-treated rats showed preference for optogenetic activation of the PVN-PFC pathway in the presence of 6g vF (**$p < 0.01$, unpaired t test; $n = 5$ ChR2 and VNS animals).
(H) CPP assay in CFA-treated rats experiencing tonic pain. Rats received light activation of PL-PFC in one chamber and no treatment in the opposite chamber.
(I) ChR2 CFA-treated rats showed preference for the chamber paired with light treatment (***$p < 0.001$, two-way ANOVA with repeated measures and Sidak's multiple comparisons test; $n = 5$ ChR2 animals).
(J) VNS CFA-treated rats showed no preference for either chamber ($p = 0.9845$, $n = 5$ VNS animals).
(K) ChR2 rats experiencing tonic pain showed preference for optogenetic activation of the PVN-PFC pathway (*$p < 0.05$, unpaired t test; $n = 5$ ChR2 and VNS animals).
(L) Spared-nerve injury (SNI) model.
(M) ChR2 rats after SNI preferred the chamber paired with light stimulation of the PVN-PFC projection (*$p < 0.05$, $n = 4$ ChR2 animals).
Data are represented as mean ± S.E.M.

KEY RESOURCES TABLE

REAGENT or RESOURCE	SOURCE	IDENTIFIER
Bacterial and Virus Strains		
pENN.AAV1.CamKII.GCaMP6f.WPRE.SV40	Addgene	Cat# 100834-AAV1; RRID: Addgene_100834
AAV1.CaMKIIa.eNpHR.3.0.EYFP	Addgene	Cat# 26791-AAV1; RRID: Addgene_26971
AAV1.CaMKIIa.EYFP	Addgene	Cat# 105622-AAV1; RRID: Addgene_105622
OTp-ChR2-mCherry	Dr. Valery Grinevich	N/A
OTp-VENUS	Dr. Valery Grinevich	N/A
OTp-hM4D(Gi)-mCherry	Dr. Valery Grinevich	N/A
hM4D(Gi) DREADD	Addgene	Cat# 50477-AAV8; RRID: Addgene_50477
CHEMICALS, PEPTIDES, AND RECOMBINANT PROTEINS		
Mycobacterium tuberculosis: Complete Freund's Adjuvant	Sigma-Aldrich	Cat# F5881–10ML
Oxytocin	Abcam	ab120186
Clozapine N-oxide	Abcam	ab141704
Vasotocin Trifluoroacetate	Bachem	4015939.0001
EXPERIMENTAL MODELS: ORGANISMS/STRAINS		
Sprague-Dawley	Taconic Farms	Model SD
SOFTWARE AND ALGORITHMS		
MATLAB R2019a	MathWorks	https://www.mathworks.com/products/matlab.html
GraphPad Prism 8	GraphPad Software	https://www.graphpad.com/scientific-software/prism/
Inscopix Data Acquisition Software	Inscopix	https://www.inscopix.com/software-analysis#software_idas
Inscopix Data Processing Software	Inscopix	https://www.inscopix.com/software-analysis#software_idps
Clampex 10.7 Software	Molecular Devices	https://support.moleculardevices.com/s/article/Axon-pCLAMP-10-Electrophysiology-Data-Acquisition-Analysis-Software-Download-Page
Constrained Nonnegative Matrix Factorization for microEndoscopic data	Open source	https://github.com/zhoupc/CNMF_E; https://doi.org/10.7554/eLife.28728.001
CellReg	Open source	https://github.com/zivlab/CellReg; Sheintuch et al., 2017
OASIS	Open source	https://github.com/zhoupc/OASIS_matlab; Friedrich et al., 2017
Gephi	Open source	https://gephi.org/

REAGENT or RESOURCE	SOURCE	IDENTIFIER
AnyMaze 5.0	Stoelting	https://stoeltingco.com/Neuroscience/Anymaze/Any-maze-Video-Tracking/Any-maze-Software
Custom code	Dr. Jing Wang's lab	https://doi.org/10.5281/ zenodo.5570672
OTHER		
nVoke 2.0	Inscopix	https://www.inscopix.com/nvoke
Gradient-index Lens	Inscopix	https://www.inscopix.com/lenses-viruses
Kwik-Sil Silicone Elastomer	World Precision Instruments	Code KWIK-SIL
Ceramic Ferrules	Thorlabs	Cat# CFLC126–10
Plantar Test	Ugo Basile	Cat# 37370
465 nm blue LED	Plexon	Cat# OPT/LED_Blue_Compact_LC_magnetic
620 nm orange LED	Plexon	Cat# OPT/LED_Orange_Compact_LC_magnetic
Carousel commutator	Plexon	https://plexon.com/products/carousel-commutator/#23rf7d84
Compact Power and Energy Meter Console, Digital "4 LCD	Thorlabs	Cat# PM100D
Transistor-transistor logic pulse generator	Doric Lenses	Code OTPG_4
Metabond Quick Adhesive Cement System	C&B	Cat# S380
Fluoromount Aqueous Mounting Medium	Sigma-Aldrich	Cat# F4680–25ML
HC-V550 Camcorder	Panasonic	https://www.panasonic.com/middleeast/en/support/product-archive/camcorder/hc-v550.html
Leica VT1000 S Vibrating Blade Microtome	Leica Biosystems	https://www.leicabiosystems.com/research/vibratomes/leica-vt1000-s/
Olympus 40x Water-Immersion Objective w/ TRITC Filter	Olympus	https://www.olympus-lifescience.com/en/objectives/lumplfln-w/